GPM Products From the Microwave-Integrated Retrieval System

Shuyan Liu, Christopher Grassotti, Junye Chen, and Quanhua Liu

***Abstract*—An updated version of the microwave-integrated retrieval system (MiRS) V11.2 was recently released. In addition to the previous capability to process multiple satellites/sensors, the new version has been extended to process global precipitation measurement (GPM) microwave imager (GMI) measurements. The main purpose of this study is to introduce MiRS GPM products and to evaluate rain rate, total precipitable water (TPW), and snow water equivalent (SWE) using various independent datasets. Rain rate evaluations were performed for January, April, July, and October 2015 which represents one full month in each season. TPW was evaluated on four days: 9 January, 1 April, 13 July, and 1 October, which represents one full day in each season. SWE was evaluated for a week in January 2015. Results show that MiRS performance is generally satisfactory in regards to both global/regional geographical distribution and quantified statistical/categorical scores. Histograms show that MiRS GPM rain rate estimates have the capability to reproduce moderate to heavy rain frequency distribution over land, and light rain distribution over ocean when compared with a ground-based reference. Evaluations of TPW show the best performance over ocean with the correlation coefficient, bias, and standard deviation of 0.99, $<$1.25 mm, and $<$2.4 mm, respectively. Robust statistical results were also obtained for SWE, with a correlation coefficient, bias, and standard deviation of 0.77, 1.72 cm, and 3.61 cm, respectively. The examples shown demonstrate that MiRS, now extended to GPM/GMI, is capable of producing realistic retrieval products that can be used in broad applications including extreme weather events monitoring, depiction of global rainfall distribution, and water vapor patterns, as well as snow cover monitoring.**

***Index Terms*—Global precipitation measurement (GPM), microwave-integrated retrieval system (MiRS), rain rate (RR), satellite.**

Manuscript received September 2, 2016; revised January 23, 2017, April 3, 2017, and May 22, 2017; accepted June 10, 2017. This work was supported by the NOAA under Grant NA14OAR4320125. *(Corresponding author: Shuyan Liu.)*

S. Liu is with the Cooperative Institute for Research in the Atmosphere, Colorado State University, Fort Collins, CO 80523 USA, and also with the NOAA Center for Satellite Application and Research, National Environmental Satellite, Data, and Information Service, College Park, MD 20740 USA. (e-mail: shu-yan.liu@noaa.gov).

C. Grassotti and J. Chen are with the Cooperative Institute for Climate and Satellites-MD/Earth System Science Interdisciplinary Center, University of Maryland, College Park, MD 20740 USA, and also with the NOAA Center for Satellite Application and Research, National Environmental Satellite, Data, and Information Service, College Park, MD 20740 USA. (e-mail: christopher.grassotti@noaa.gov; junye.chen@noaa.gov).

Q. Liu is with the NOAA Center for Satellite Application and Research, National Environmental Satellite, Data, and Information Service, College Park, MD 20740 USA. (e-mail: quanhua.liu@noaa.gov).

Color versions of one or more of the figures in this paper are available online at http://ieeexplore.ieee.org.

Digital Object Identifier 10.1109/JSTARS.2017.2716356

I. Introduction

Satellite-based observations have provided expanded opportunities for rainfall and hydrometeor monitoring by providing global-scale brightness temperature measurements over land and ocean. Accurate rain rate retrieval around the globe is crucial for applications, such as extreme weather event detection, flood, and drought monitoring. Retrieval techniques based on space-based measurements began in 1970s when meteorological satellites became operational in greater number and began transmitting radiance data back to the Earth [1]. Due to the advantages of high spatial and temporal coverage relative to ground-based measurements, such as radar and rain gauge, many algorithms have been developed to convert satellite measured radiances into geophysical parameters, including precipitation.

By estimating the direct interaction of the radiation with liquid and frozen water in the atmospheric column, data from microwave radiometers, thus, can be used to provide physically reasonable retrievals of precipitation rate. Wilheit *et al.* [2] comprehensively examined 16 rainfall intensity retrieval algorithms including algorithms that use high-frequency scattering measurements, low-frequency emission measurements, and combinations based on the special sensor mircrowave imager radiances. Weng *et al.* [3] and Ferraro *et al.* [4] described the microwave surface and precipitation product system which retrieves total precipitable water (TPW), cloud liquid water, and ice water path using a physical approach, and evaluated the product based on multiple sensors. The advantages of statistical regression-based algorithms are 1) they do not require knowledge of the physical relationship between rain rate and satellite brightness temperature, and 2) assuming there exists a linear relationship between brightness temperatures and rainfall, they always minimize the least squares retrieval error. However, the relationship between rain rate and microwave radiances is known to be highly nonlinear, as well as exhibit seasonal and regional dependence. Thus, a physical-based retrieval algorithm was introduced by Petty [5] aimed at inverting multichannel microwave radiances to determine physical information on hydrometeors. In addition to rain, Surussavadee and Staelin [6] extended the retrievals to snowfall rate and to snow and ice surfaces. The Goddard Profiling Algorithm is a noteworthy system which uses a Bayesian inversion for all surface types. The method was first developed to retrieve precipitation from the tropical rainfall measuring mission microwave imager [7], and then evolved to a fully parametric approach used operationally on global precipitation measurement (GPM) microwave imager (GMI) [8].

The microwave-integrated retrieval system (MiRS, https://www.star.nesdis.noaa.gov/mirs/) is an inversion algorithm based on physical forward modeling and can invert observed multichannel radiances simultaneously to determine key components of the atmosphere and surface state, including rain parameters [9], [10]. The system has been operational since 2007 at the National Oceanic and Atmospheric Administration (NOAA) and has routinely produced satellite retrieval products from a growing list of microwave satellites/sensors. The most recent released version is V11.2 which extended MiRS capability to process GPM/GMI measurements. This study introduces and evaluates GPM/GMI retrieval products within the MiRS framework. Section II introduces 1) the MiRS algorithm, 2) the GPM/GMI data used as input to the system, 3) other datasets that were used as references to estimate performance, and 4) the performance evaluation methods. Section III includes MiRS-retrieved products and evaluation results. Discussion and conclusion are in Section IV.

II. Algorithm, Data, and Evaluation Method

The MiRS is an iterative physically-based one-dimensional variational (1-DVAR) retrieval algorithm [11], [12]. The principle is to minimize a two-term penalty function, which is composed of the departure of the simulated radiances from measurements and the departure of the retrieved parameters from their respective *a-priori* backgrounds. To evaluate MiRS-GPM/GMI products, we used various independent data for different parameters, i.e., Stage-IV radar-gauge composites for rain rate (RR), European Centre for Medium-Range Weather Forecasts (ECMWF) global analyses for TPW, and Japan Aerospace Exploration Agency (JAXA) advanced microwave scanning radiometer 2 (AMSR2) data for snow water equivalent (SWE).

A. MiRS Algorithm

The 1-DVAR algorithm used by MiRS is an iterative approach finding the optimal solution that fits the observed satellite radiance, subject to other constraints. The cost function to be minimized is

$$J(X) = \left[\frac{1}{2}(X - X_0)^T \times B^{-1} \times (X - X_0)\right] + \cdot \left[\frac{1}{2}(Y^m - Y(X))^T \times E^{-1} \times (Y^m - Y(X))\right] \tag{1}$$

where *X* is the retrieved state vector. The first item on the right represents the penalty for departing from background X_0 weighted by the error covariance matrix *B*. The second term represents the penalty for the simulated radiances *Y* departing from the observed radiances Y^m, weighted by instrument and modeling error *E*.

Assuming local linearity

$$y(x) = y(x_0) + K[x - x_0]. \tag{2}$$

This leads to iterative solution

$$\Delta X_{n+1} = \left\{BK_n^T\left(K_n B K_n^T + E\right)^{-1}\right\} \cdot \left[(Y^m - Y(X_n)) + K_n \Delta X_n\right] \tag{3}$$

where ΔX is the increment of the state vector iteration $n + 1$, and *K* is the matrix of Jacobian which contains the sensitivity of the radiances to changes in X (parameters to retrieve).

The departure from measured radiances normalized by the noise level and the specification of uncertainty in the forward modeling make it possible to use the signal of a particular channel when the geophysical signature is stronger than the noise. Conversely, at other times, it may be possible to deweight the information from same channel when the signal in question is within the noise level. The departure from the background scaled by the uncertainty assigned to the background result in retrievals closer to an *a-priori* background estimate if it is deemed accurate. The MiRS currently uses a "dynamic background" as an *a-priori* constraint, for temperature, water vapor, and skin temperature, which varies with latitude, longitude, season, and time of day. Empirical orthogonal functions are used as basis functions to further reduce the degrees of freedom in the solution and stabilize the retrieval.

The Community Radiative Transfer Model (CRTM) [13], [14] produces radiances and the corresponding Jacobians under clear, cloudy, and precipitating conditions. The model has been validated against various satellite measurements [15], [16]. MiRS uses CRTM as the forward operator to perform retrievals under all these sky conditions. Given a set of radiances, an *a-priori* (background) estimate of the geophysical mean and its associated covariance matrix, and assuming the hypotheses for its mathematical basis are satisfied, MiRS produces a set of self-consistent parameters that are also consistent with the measured parameters. When processing satellite sensor data with a full complement of temperature, water vapor, and surface-sensitive channels, the official MiRS products generally include temperature and water vapor vertical profiles, cloud and precipitation vertical profiles (nonprecipitating cloud amount, rain, and graupel), skin temperature, and the surface emissivity spectrum. Postprocessing of elements within the retrieved state vector yield additional retrieval products, such as RR, TPW, sea ice concentration and age, SWE, and grain size. In the case of TPW, simple vertical integration of the retrieved water vapor profile is done. For RR, offline relationships between surface RR and total rain water, graupel water, and cloud liquid water path were developed from mesoscale forecast model simulations. Finally, for sea ice and snow water, external catalogs that relate the surface emissivity spectrum to ice and snow amounts are used. In the case of snow water, a single-layer physical snow model developed at NOAA is used to build the catalogs. An important feature of MiRS is that, as currently configured, retrievals do not require real-time ancillary data such as those coming from numerical weather prediction model forecasts. MiRS products based on various satellite/sensors have been examined, for example, [17], [18]. In the case of GPM/GMI, with a reduced channel set primarily designed to measure surface and precipitation phenomena, the official MiRS GPM products are RR, rain water path, graupel water path, cloud liquid water, TPW, and SWE.

B. Datasets Description

The GPM satellite, launched on February 27, 2014, is a joint effort of JAXA and the National Aeronautics and Space Administration. GPM has dual-frequency precipitation radar and GMI passive radiometer onboard. This study uses GMI observed microwave radiances as input to MiRS. GMI, across a swath of 885 km, is a passive sensor that uses 13 different frequency/polarization channels to observe energy from various types of precipitation through clouds for estimating everything from heavy to light rain and for detecting falling snow. Table I lists GMI channel information, including central frequency, polarization, bandwidth, noise equivalent differential temperature (NEDT), beam width, and ground footprint size. Retrieved output products from MiRS analyzed in this study include the surface RR as well as rain water, graupel water, and nonprecipitating cloud water. This paper will evaluate RR, TPW, and SWE with different independent data sources.

RR retrievals are evaluated by Stage IV [19], [20] which is a 4-km gridded precipitation analysis over the conterminous U.S. (CONUS) produced by National Centers for Environmental Prediction. The data are based on the multisensor precipitation estimator analyses known as Stage III which use multisensor data (WSR-88D radar and gauges) and are specified on 4-km polar-stereographic grids produced by the 12 River Forecast Centers. In this paper, we used the hourly products that are collocated with GPM/GMI measurements for validation. The ECMWF (http://www.ecmwf.int/) data which are used to evaluate MiRS performance have 91 vertical levels between the surface and 0.01 hPa. The horizontal resolution is approximately 125 km (spectral truncation T159) and the temporal resolution is 3 h. The ECMWF gridded data were matched to sensor granules for direct comparison. MiRS retrieved SWE was compared with the Level-3 SWE dataset based on observations of AMSR2 [21] onboard JAXA Global Change Observation Mission 1st-Water (GCOM-W) June 2015 and were mapped to 25-km grids in near real-time mode (available at https://lance.nsstc.nasa.gov/amsr2-science/data/level3/daysnow/).

C. Evaluation Methods

Performance of the retrieval system was evaluated both objectively by statistical and categorical scores and subjectively by viewing geographical distribution. Statistical evaluation includes correlation coefficients, biases, standard deviations, and root–mean-square errors. In this study, we use three categorical scores [22] to evaluate RR retrieval. Probability of detection (POD), sometimes called hit rate, represents the ratio of total rain retrievals greater than a threshold divided by total rain observations in Stage IV greater than the same threshold and defined by: POD = (number of rain events correctly retrieved by MiRS)/(total number of Stage-IV observed rain events). False alarm ratio (FAR), the fraction of the all observed no rain events (as defined by a threshold) in which there was a retrieval of rain greater than the same threshold, and is calculated by: FAR = (number of retrieved false alarms)/(total number of Stage IV no rain events). (Note that this is defined in [22] as the Probability of false detection.) The Heidke skill score (HSS) measures the fraction of correct rain retrieval after eliminating those retrievals which would be correct due purely to random chance. Thus, HSS = (correct retrieval proportion−proportion correct by chance)/(total number of observations−proportion correct by chance), in which a perfect score = 1.

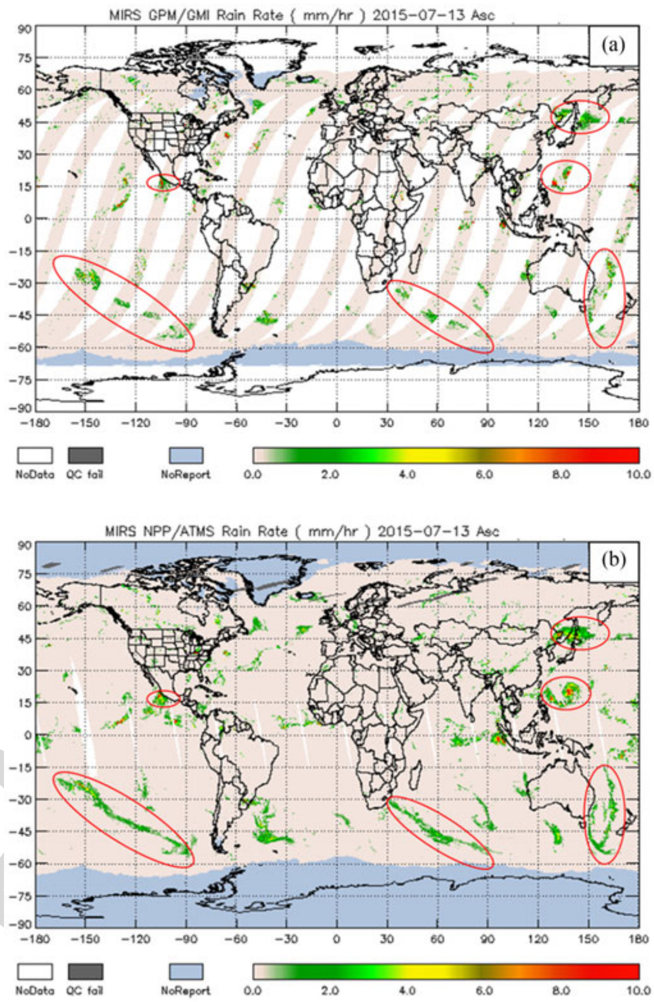

Fig. 1. Global RR distribution intercomparision between (a) MiRS GPM/GMI and (b) SNPP/ATMS for July 13, 2015.

III. Results

The global RR distribution retrieved by MiRS GPM/GMI for July 13, 2015 is shown in Fig. 1(a). MiRS retrievals based on the advanced technology microwave sounder (ATMS) onboard the Suomi national polar-orbiting partnership (SNPP) are also included for an intercomparison (see Fig. 1(b)). MiRS does not retrieve RR over frozen surfaces; thus, the northern and southern snow and sea ice covered areas are denoted as no reports for SNPP/ATMS (see Fig. 1(b)). Despite the swath gaps, GPM/GMI is consistent in distribution and intensity with SNPP/ATMS globally. Active rain areas (red circle on the figures), such as adjacent ocean of southern Mexico and Northern Japan, Philippine

TABLE I
GPM/GMI CHANNEL INFO

Chan. No.	Central Freq. (GHz) (Polarization)	Band Width (MHz)	NEDT[a] (K)	Beam Width (deg)	FOV[b] size AS[c] $\times$ CS[d] (km)
1	10.65 (V)	100	0.96	1.75	19.4 × 32.2
2	10.65 (H)	100	0.96	1.75	19.4 × 32.2
3	18.7 (V)	200	0.84	1.00	11.2 × 18.3
4	18.7 (H)	200	0.84	1.00	11.2 × 18.3
5	23.8 (V)	400	1.05	0.90	9.2 × 15
6	36.5 (V)	1000	0.65	0.90	8.6 × 14.4
7	36.5 (H)	1000	0.65	0.90	8.6 × 14.4
8	89.0 (V)	6000	0.57	0.40	4.4 × 7.3
9	89.0 (H)	6000	0.57	0.40	4.4 × 7.3
10	166.0 (V)	3000	1.5	0.40	4.4 × 7.1
11	166.0 (H)	3000	1.5	0.40	4.4 × 7.1
12	183.31 ± 3 (V)	3500	1.5	0.40	4.4 × 7.2
13	183.31 ± 7(V)	4500	1.5	0.40	4.4 × 7.2

[a]NEDT: Noise equivalent differential temperature.
[b]FOV: Field-of-view.
[c]AS: Along-scan direction.
[d]CS: Cross-scan direction.

TABLE II
LAND RR STATISTICAL ANALYSES OVER CONUS

Month	No. of Points ($\times 10^3$)	Corr. Coef.	Bias (mm/h)	Std. Dev. (mm/h)
January	1390	0.60	−0.02	0.58
April	2567	0.55	0.03	0.86
July	2733	0.52	0.04	1.18
October	2662	0.58	0.01	0.70

Sea, the Southern Hemisphere ocean around −45° latitude, etc., are consistent across the two satellite retrievals. There are some inconsistencies between the two due to different local passing time. The SNPP is in a geosynchronous polar orbit with a local equatorial passing time of 1:30 pm (ascending), while GPM orbits between 65°N and 65°S, and does not have a fixed passing time, but one that repeats approximately every two weeks.

RR retrieval performance at the hourly timescale has been quantified for four full months chosen to reflect the typical seasonal cycle over the Northern Hemisphere, which in this study were January, April, July, and October from 2015. Table II contains the statistics based on collocation over the CONUS with the hourly Stage IV analyses over land surfaces. Correlations between land retrievals and observations for January, April, July, and October are 0.60, 0.55, 0.52, and 0.58, biases are −0.02, 0.03, 0.04, and 0.01 mm/h, and the standard deviations are 0.58, 0.86, 1.18, and 0.70 mm/h, respectively.

To characterize the distribution of RR, histograms based on over land rainfall are shown in Fig. 2, for each of the four months. Over land, MiRS typically underestimates relative to Stage IV the occurrence of light rain events below 2.0 mm/h for all four months (see Fig. 2(a)–(d)) with January and July showing the maximum and minimum underestimation, respectively. The seasonal transition months of April and October show similar behavior, lying in between the two extremes of January and July. Above approximately 2 up to 10 mm/h, agreement between MiRS and Stage IV occurrence is quite good in all four months. The underestimation of light rain occurrence over land is characteristic of microwave retrieval algorithms generally, as the emission signal of the rainfall is low relative to the high and variable surface emission background.

We further calculated categorical scores of POD, FAR, and HSS as a function of rain/no rain threshold at 0.5-mm/h intervals. The results are shown in Fig. 3. POD and HSS for the four months are generally higher than 0.3. In July, both POD and HSS are highest at the lowest RR threshold (0.5 mm/h). This is likely due to the climatological presence of low-level stratiform rain in fall, winter, and spring, which can be contrasted with July in which light rainfall may have origins with deeper convective systems having a stronger scattering signal in microwave measurements. Comparing with summer (July) which shows almost linear deceasing scores from light to heavy rain, winter (January) POD, and HSS peaked at 2 mm/h. During spring (April) and fall (October), both PODs have the highest value at 2 mm/h, HSS in April is decreasing with increasing RR while in October is stable between 0.35 and 0.40.

RR retrieval at the regional and monthly scale is illustrated over the CONUS (seeFig. 4) for land surfaces for the same four months in 2015. RR retrievals from GPM were collocated with Stage IV hourly estimates for each day of the month to produce a monthly accumulated rainfall on the Stage IV 4-km grid. (Note that this is not the true monthly accumulation since any location would be sampled at most twice daily by GPM, and because the Stage IV analyses are not reliable for many locations in the mountainous western U.S. due to orographic artifacts in the required radar data [23].) Monthly accumulated rain retrieval along GPM swaths (see Fig. 4(a)–(d)) for January, April, July, and October 2015 is compared with collocated Stage-IV grids (see Fig. 4(e)–(h)). In each map, the areas masked in white over the western U.S. are locations where the Stage IV processing does not estimate rainfall due to radar beam blockage effects. The comparison statistics for the over land estimates are also shown for each month. Generally, the MiRS rainfall retrievals capture major characteristics of the monthly precipitation geographic distribution seen in Stage IV. In January, for example, MiRS GPM and Stage-IV agree very well over the southern

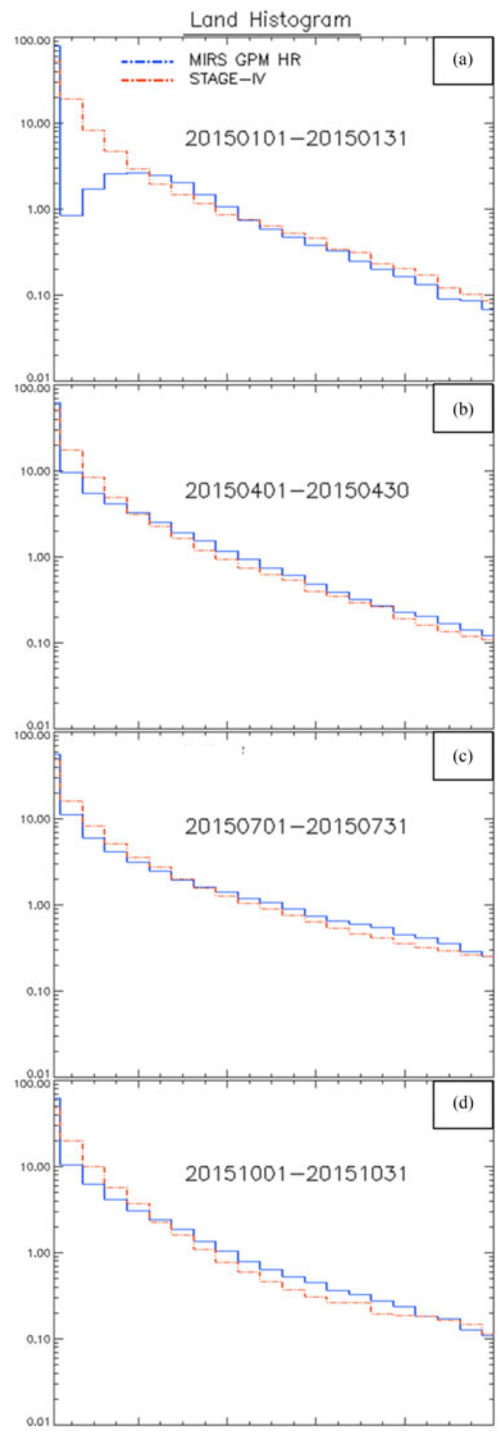

Fig. 2. RR histograms as a function of rain/no rain threshold validated against Stage IV over land for the months of (a) January 2015, (b) April 2015, (c) July 2015, and (d) October 2015.

Gulf Coast states from Texas eastward to the Florida panhandle. Further northward, there is a tendency of the MiRS rainfall to underestimate the totals seen in Stage IV, which is consistent with known difficulties of satellite algorithms to detect and estimate lighter stratiform rainfall common in the cold season (see also Fig. 2(e)–(h)). In the warmer seasons, particularly April and July, the MiRS and Stage IV totals are in fairly good agreement, with some indication that the MiRS amounts at the higher end of the distribution (>100 mm) are more prevalent than those in the Stage IV. The other noticeable feature is the presence during some months of spurious high rainfall amounts at major coastlines and also along some lakeshores such as the Great Lakes. This is due to the presence of mixed surface types within the GMI microwave footprints which are difficult to characterize. Due to the inherently larger size of the measurement footprint relative to infrared observations, microwave rainfall retrieval algorithms often have difficulty with coastlines and many algorithms do not produce estimates if a coastline is detected. The range of comparison statistics over the four months for correlation, bias (mm), and standard deviation (mm) are [0.45, 0.58], [−1.73, 4.25], and [17.6, 28.6], respectively. Total collocation points ranged from 310 289 in January to 404 523 in October.

Finally, it is important to note that the Stage IV data are known to have limitations since radar to RR relationships themselves contains uncertainties and the algorithms used at River Forecast Centers have certain biases. For example, uncertainties increase in the case of light rain detection during winter season generally, and over the Western U.S. as a result of fewer radar locations and mountain beam blockage [24]. This could have the effect of spuriously elevating false alarms and lowering other skill scores when the satellite estimate has correctly identified precipitation.

TPW retrieved from MiRS GPM/GMI was evaluated by comparing with collocated ECMWF analyses. Bias maps from one day in each season, i.e., 9 January, 1 April, 13 July, and 1 October 2015 were shown to illustrate the spatial dependence of retrieval performance (see Fig. 5). In comparison with ECMWF, MiRS generally depicts the geographical distribution of TPW well with larger biases over land than over ocean, snow, and ice for all four days due, in part, to larger uncertainties in land surface emissivity. Thermally cold surfaces have smaller and positive biases than warm surfaces, e.g., the northern hemisphere land compared to the southern hemisphere in January. Northern South America show dry biases all four days, as well as Australia in January and April. For 13 July, TPW over the northern hemisphere land has noticeably large negative biases.

Statistical analyses for land, ocean, snow, and ice surface types were performed separately (see Table III). Among all the surface types, ocean has the highest correlation coefficients of 0.99 regardless of day. Consistent with Fig. 5, land retrievals typically have negative (dry) biases, while other surfaces are smaller and positive. Land and ocean retrievals generally have the highest correlation coefficients, while snow and ice generally show lower correlations. The highly variable nature of cryospheric surface emissivities in space and time, generally contribute to increased uncertainty in retrievals over these surfaces.

Since the MiRS algorithm is run without the use of ancillary data (e.g., NWP-based analyses or forecasts), and since GPM/GMI does not have the full set of temperature sounding channels, it is expected that the water vapor retrievals will have larger uncertainties when compared with measurements from, for example, SNPP/ATMS. Further work on tuning and optimizing some of the constraints in the retrieval system (e.g., atmospheric and surface covariances, radiometric bias

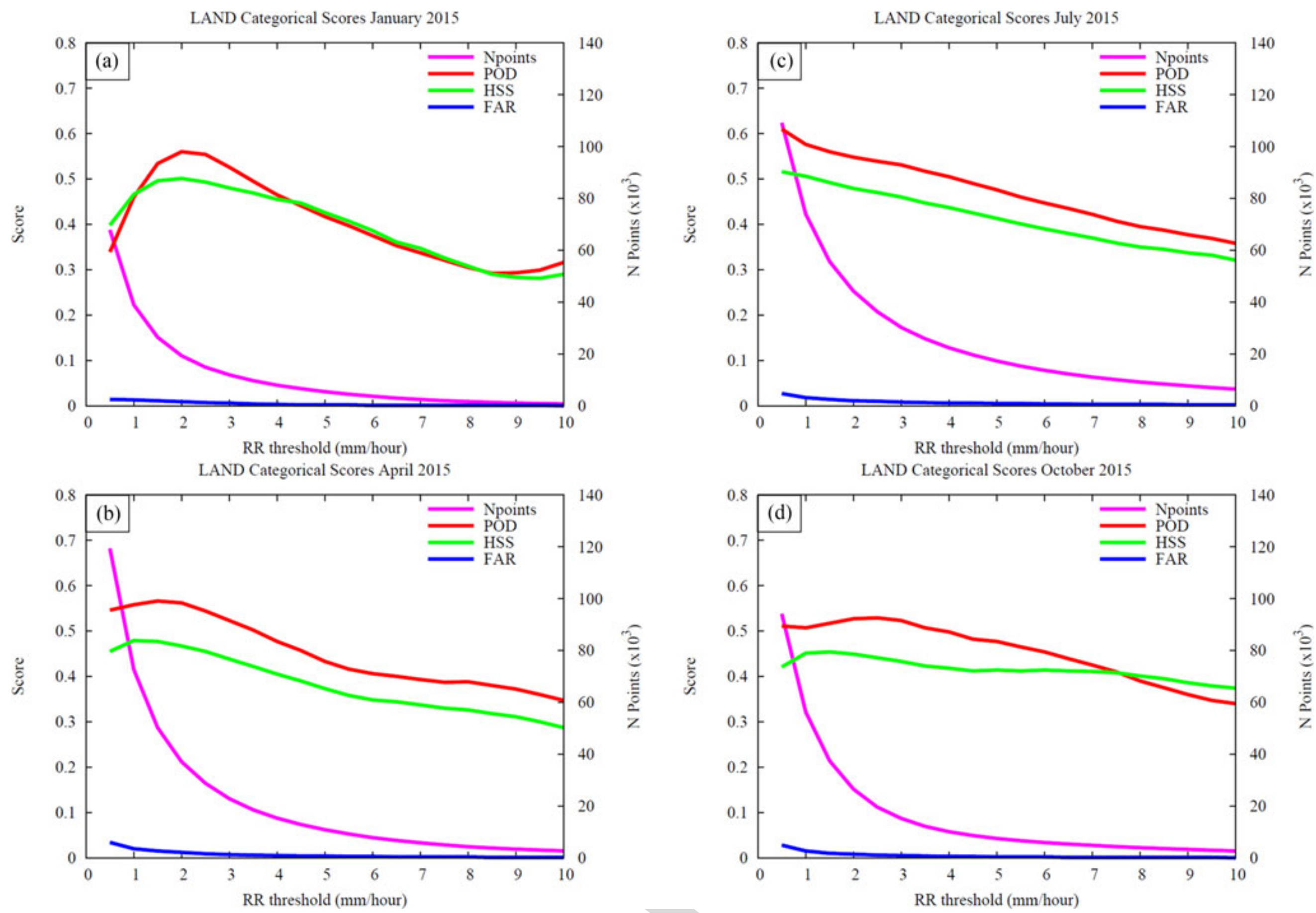

Fig. 3. RR categorical scores as a function of rain/no rain threshold validated against Stage IV over land for the months of (a) January 2015, (b) April 2015, (c) July 2015, and (d) October 2015.

corrections, empirical orthogonal function basis functions) may mitigate some of the biases and uncertainties seen in the retrieved TPW, particularly over land.

Performance of SWE over the northern hemisphere retrievals is shown in Fig. 6. Fig. 6(a) illustrates the northern hemisphere spatial distribution of the MiRS GPM SWE for January 5, 2015, while Fig. 6(b) contains the corresponding map from the independent reference dataset of GCOM-W/AMSR2 SWE, based on the JAXA algorithm. Fig. 6(c) is the density scatter plot of MiRS GPM retrievals and the AMSR2 SWE for one week period of January 4–10, 2015. The two daily maps indicate that in areas with very high SWE, for example, eastern Russia and Siberia, the MiRS GPM estimates tend to be larger than the JAXA AMSR2 estimates, while in areas with lower SWE amounts (<10 cm), for example, Southern Canada and Europe, the MiRS estimates tend to be lower than JAXA AMSR2. Since both products are based on remotely sensed data, it is difficult to state with confidence which estimates may be more accurate. Factors such as snow grain size, forest cover (which tends to mask the underlying snow signal), and local time of observation (which can affect local temperature, and, hence, snow wetness) are all sources of uncertainty in microwave SWE estimates. The scatter plot for the seven-day period shows a distribution of points close to the 1:1 line with a correlation coefficient value of 0.77. Overall, MiRS retrievals are systematically higher than the JAXA AMSR2 estimates (with the regional exception noted above over Asia for the single day). The bias and standard deviation are 1.7 and 3.6 cm, respectively. Comparison statistics for each individual day (not shown) indicate that the results are quite stable and quite close to the aggregate statistics from the one week of processed data. The correlation coefficient ranged from 0.76 to 0.79, bias ranged from 1.5 to 2.2 cm, and standard deviation from 3.6 to 3.7 cm.

IV. Discussion and Summary

MiRS is a robust flexible satellite retrieval system designed for rapid physically-based atmospheric and surface property retrievals from passive microwave measurements. The MiRS algorithm has been running operationally at NOAA since 2007 and routinely distributing satellite derived products through NOAA Office of Satellite and Product Operations. The system is now processing multiple satellites/sensors, i.e., AMSUA and MHS onboard NOAA-18, NOAA-19, MetopA, and MetopB which are polar-orbiting operational environmental satellites; ATMS onboard SNPP satellite; special sensor microwave imager/sounder onboard defense meteorological satellite program satellites F-17 and F-18; and sounder for probing vertical profiles of humidity onboard Megha-Tropiques.

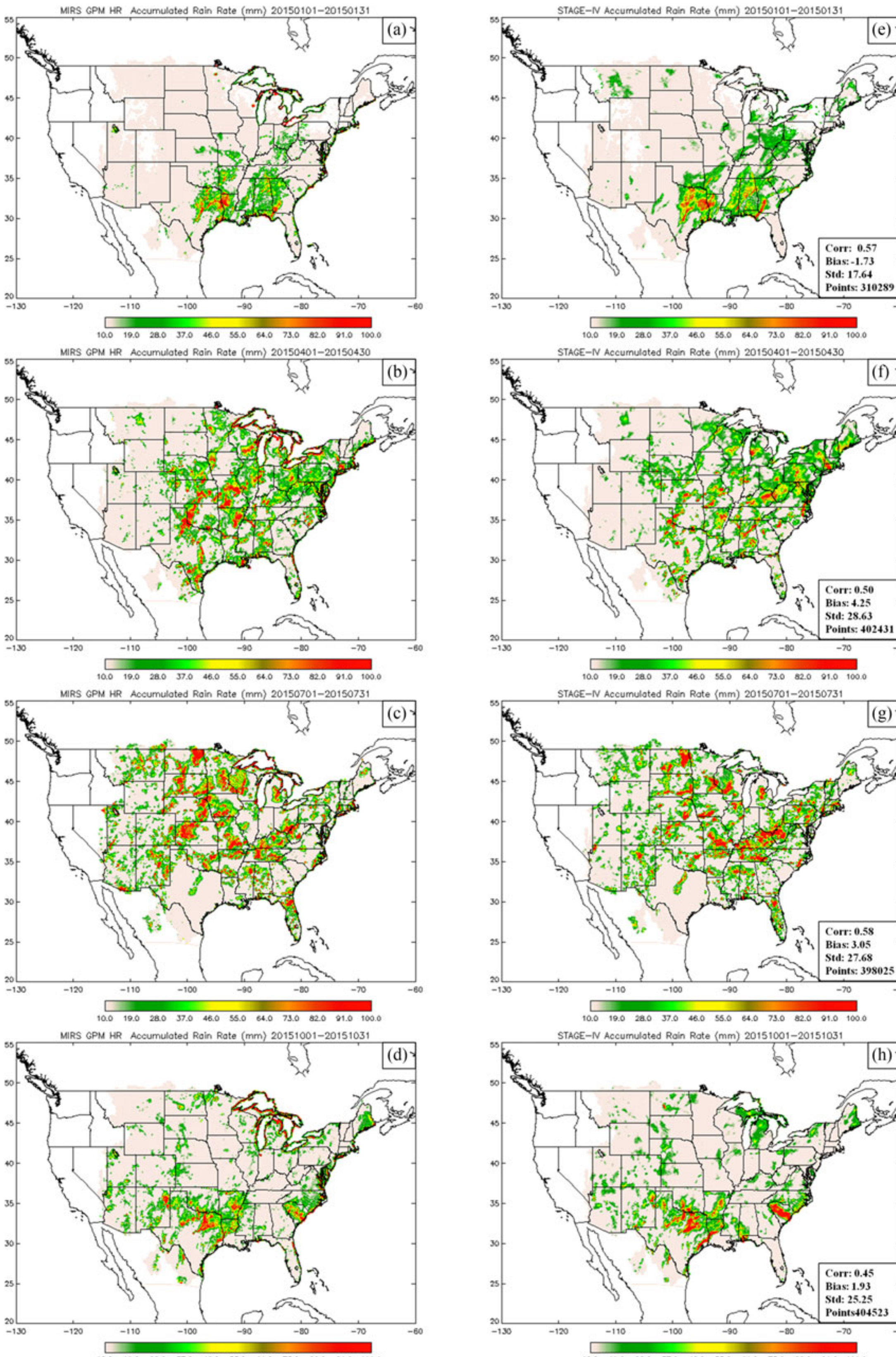

Fig. 4. Accumulated rain (mm) from MiRS GPM/GMI (left panels) and observations from collocated Stage IV (right panels) for the months of (a) and (e) January, (b) and (f) April, (c) and (g) July, and (d) and (h) October 2015. Areas in western U.S. are missing since no Stage IV estimates were produced over these regions. Areas over Rocky Mountains and northern U.S. in January are missing due to frequent snow cover during which MiRS does not produce a rain retrieval.

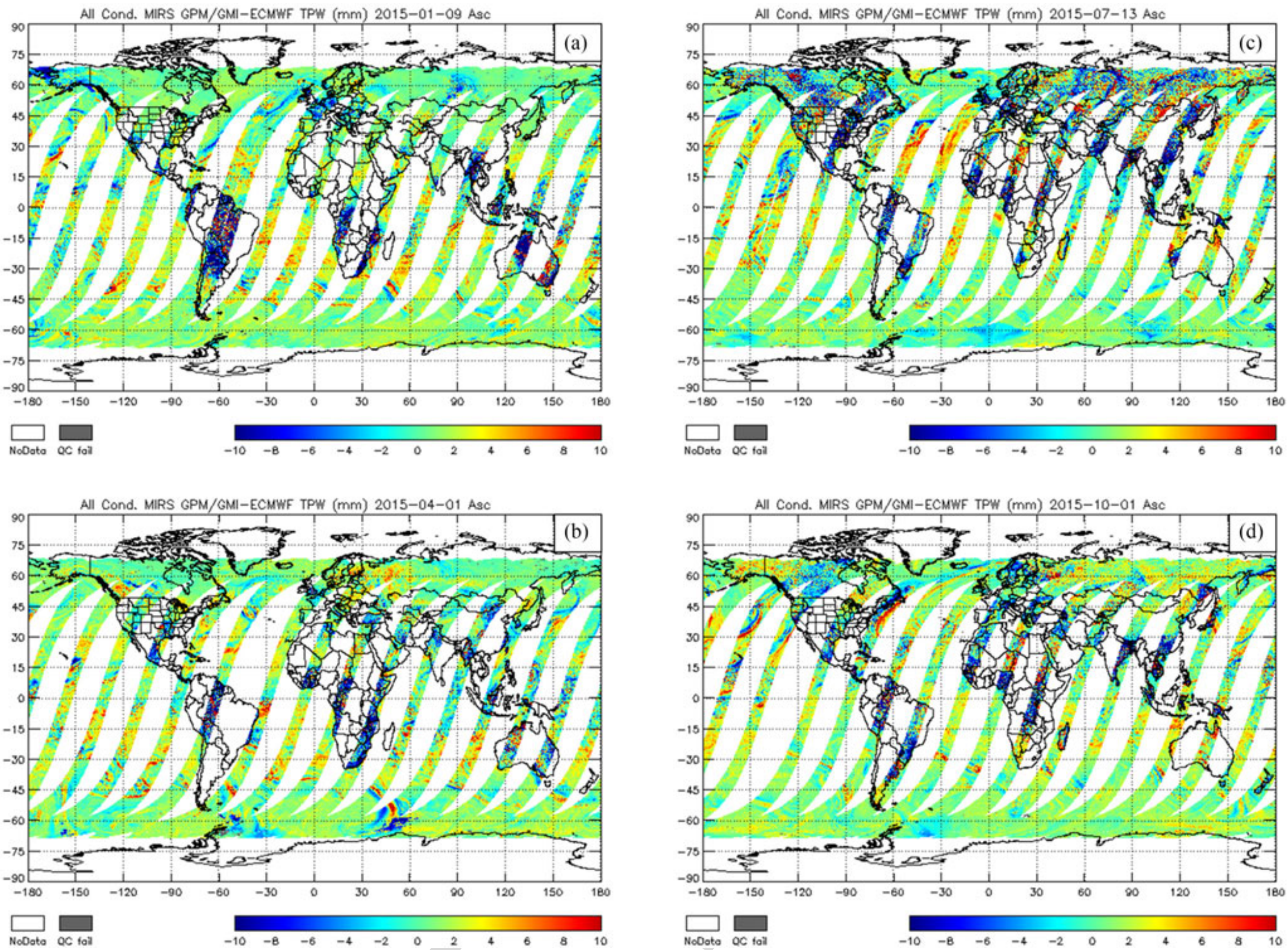

Fig. 5. Geographical distribution of total precipitable water (TPW) biases uses ECMWF as reference for (a) January 9, 2015, (b) April 1, 2015, (c) July 13, 2015, and (d) October 1, 2015.

TABLE III
CLEAR SKY TPW STATISTICAL ANALYSES

Surface Surface	Date Date	No. of Points ($\times 10^3$)	Corr. Coef.	Bias (mm)	Std. Dev. (mm)
Land	2015-01-09	604	0.92	−2.53	6.89
	2015-04-01	542	0.91	−1.76	5.99
	2015-07-13	830	0.83	−1.60	7.04
	2015-10-01	784	0.90	−1.16	6.27
Ocean	2015-01-09	1557	0.99	1.17	2.21
	2015-04-01	1559	0.99	1.17	2.31
	2015-07-13	1534	0.99	1.11	2.38
	2015-10-01	1502	0.99	1.24	2.17
Snow	2015-01-09	458	0.86	0.36	1.44
	2015-04-01	348	0.82	0.72	1.62
	2015-07-13	26	0.82	0.89	3.05
	2015-10-01	57	0.66	1.23	2.53
Ice	2015-01-09	138	0.74	0.29	2.46
	2015-04-01	114	0.72	0.13	2.59
	2015-07-13	234	0.91	0.11	1.97
	2015-10-01	277	0.85	0.84	1.55

The most recent version (v11.2) has been extended to GPM/GMI. This study is intended as an introductory quantitative assessment of the MiRS GPM retrieval products of RR, TPW, and SWE using independent datasets. Global and regional CONUS geographical distribution of surface precipitation is in good qualitative agreement with SNPP/ATMS retrievals and with the operational Stage-IV analyses. Quantitative evaluation based on four months (one full month in each season) showed that MiRS GPM RR performance is consistent with that seen for MiRS RR from other operational satellites. TPW distribution is consistent with ECMWF globally with higher biases over land than over ocean based on the four days (one day in each season) of evaluation. As expected, among the four surface types, ocean TPW has the best performance. This is consistent with TPW performance seen from MiRS for other sensors and from other microwave algorithms. SWE over northern hemisphere was compared with the corresponding product based on AMSR2. Point to point comparison indicates good agreement between the two.

Further investigations are underway including 1) evaluating the impact of assumed radiometric uncertainty in each channel, 2) influence of each assumed *a-priori* hydrometeor background constraints, 3) possible implementation of an *a-priori* temperature and water vapor error covariance matrix specific to rainy conditions, 4) exploring methods to distinguish convective and stratiform (or mixed) precipitation types using, when available,

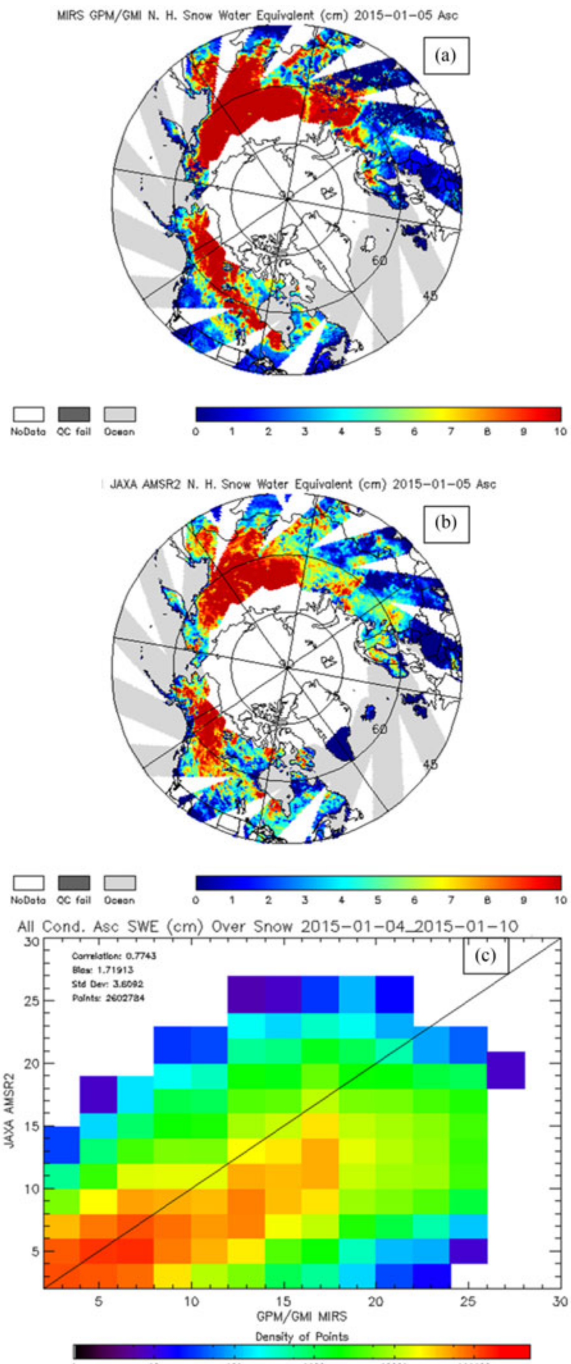

Fig. 6. SWE distribution over the northern hemisphere retrieved from (a) MiRS GPM, (b) AMSR2 retrieval from JAXA algorithm for January 5, 2015, and (c) density scatter plot for one week of January 4–10, 2015.

signal differences between measurements in vertical and horizontal polarization, and 5) use of an air mass-dependent set of radiometric bias corrections instead of the current static corrections. One of the important features of MiRS is that when run in operations, it does not use any ancillary data. External data for the surface (especially emissivity) from climatology or for the atmosphere (water vapor, temperature) from numerical weather prediction systems is anticipated to be beneficial to the retrieval products, but needs to be quantified. Another improvement path in MiRS is that particle size assumptions in CRTM may not be optimal for all precipitation types (e.g., seasonal, regional, stratiform versus convective). Finally, the impact of updated scattering tables (to be available in upcoming versions of CRTM) that account for the effects of nonspherical particles will need to be evaluated.

ACKNOWLEDGMENT

This paper contents are solely the opinions of the authors and do not constitute a statement of policy, decision, or position on behalf of NOAA or the U.S. Government.

REFERENCES

[1] P. A. Arkin and B. N. Meisner, "The relationship between large-scale convective rainfall and cold cloud over the western hemisphere during 1982-84," *Monthly Weather Rev.*, vol. 115, no. 1, pp. 51–74, Jan. 1987.

[2] T. T. Wilheit *et al.*, "Algorithms for the retrieval of rainfall from passive microwave measurements," *Remote Sens. Rev.*, vol. 11, nos. 1–4, pp. 163–194, Oct. 2004.

[3] F. Weng, L. Zhao, R. R. Ferraro, G. Poe, X. Li, and N. C. Grody, "Advanced microwave sounding unit cloud and precipitation algorithms," *Radio Sci.*, vol. 38, no. 4, pp. 8068–8081, Mar. 2003, doi:10.1029/2002RS002679.

[4] R. R. Ferraro *et al.*, "NOAA operational hydrological products derived from the advanced microwave sounding unit," *IEEE Trans. Geosci. Remote Sens.*, vol. 43, no. 5, pp. 1036–1049, May 2005, doi:10.1109/TGRS.2004.843249.

[5] G. W. Petty, "Physical retrievals of over-ocean rain rate from multichannel microwave imagery. Part II: Algorithm implementation," *Meteorol. Atmos. Phys.*, vol. 54, nos. 1–4, pp. 101–121, Mar. 1994.

[6] C. Surussavadee and D. H. Staelin, "Satellite retrievals of arctic and equatorial rain and snowfall rates using millimeter wavelengths," *IEEE Trans. Geosci. Remote Sens.*, vol. 47, no. 11, pp. 3697–3707, Nov. 2009.

[7] C. D. Kummerow *et al.*, "The evolution of the goddard profiling algorithm (GPROF) for rainfall estimation from passive microwave sensors," *J. Appl. Meteorol.*, vol. 40, no. 11, pp. 1801–1820, Nov. 2001.

[8] C. D. Kummerow *et al.*, "The evolution of the goddard profiling algorithm to a fully parametric scheme," *J. Atmos. Ocean. Technol.*, vol. 32, pp. 2265–2280, Dec. 2015.

[9] S.-A. Boukabara, F. Weng, and Q. Liu, "Passive microwave remote sensing of extreme weather events using NOAA-18 AMSUA and MHS," *IEEE Trans. Geosci. Remote Sens.*, vol. 45, no. 7, pp. 2228–2246, Jul. 2007.

[10] S.-A. Boukabara *et al.*, "MiRS: An all-weather 1DVAR satellite data assimilation & retrieval system," *IEEE Trans. Geosci. Remote Sens.*, vol. 49, no. 9, pp. 3249–3272, Sep. 2011, doi:10. 1109/TGRS.2011.2158438.

[11] C. D. Rodgers, *Inverse Methods for Atmospheric Sounding: Theory and Practice*. Singapore: World Scientific, 2000.

[12] Q. Liu and F. Weng, "One-dimensional retrieval algorithm of temperature, water vapor, and cloud water profiles from advanced microwave sounding unit (AMSU)," *IEEE Geosci. Remote Sens.*, Seoul, Korea, vol. 43, no. 5, pp. 1087–1095, 2005.

[13] F. Weng *et al.*, "JCSDA community radiative transfer model (CRTM)," in *Proc. 14th TOVS Conf.*, Beijing, China, 2005, pp. 217–222.

[14] Y. Han *et al.*, "Community radiative transfer model (CRTM)," Dept. Commerce, NOAA, Washington, DC, USA, Tech. Rep. 122, 2006.

[15] Y. Chen, F. Weng, Y. Han, and Q. Liu, "Validation of the community radiative transfer model (CRTM) by using CloudSat data," *J. Geophys. Res.*, vol. 113, no. D8, pp. 2156–2202, 2008.

[16] S. Ding *et al.*, "Validation of the community radiative transfer model," *J. Quant. Spectrosc. Radiat. Transf.*, vol. 112, no. 6, pp. 1050–1064, 2011.

[17] S.-A. Boukabara *et al.*, "A physical approach for a simultaneous retrieval of sounding, surface, hydrometer, and cryospheric parameters from SNPP/ATMS," *J. Geophys. Res. Atmos.*, vol. 118, no. 12, pp. 12 600–12 619, 2013, doi:10.002/2013JD020448.

[18] F. Iturbide-Sanchez *et al.*, "Assessment of a variational inversion system for rainfall rate over land and water surfaces," *IEEE Trans. Geosci. Remote Sens.*, vol. 49, no. 9, pp. 3311–3333, Sep. 2011, doi:10.1109/TGRS.2011.2119375.

[19] M. E. Baldwin and K. E. Mitchell, "Progress on the NCEP hourly multi-sensory U.S. precipitation analysis for operations and GCIP research," in *Proc. Amer. Meteor. Soc. 2nd Symp. Integr. Obs. Syst.*, Phoenix, AZ, USA, 1998, pp. 54–55.

[20] Y. Lin and K. E. Mitchell, "The NCEP stage II/IV hourly precipitation analyses: Development and applications," in *Proc. Amer. Meteor. Soc. 19th Conf. Hydrol.*, San Diego, CA, USA, 2005, Paper 1.2. [Online]. Available: http://ams.confex.com/ams/Annual2005/techprogram/paer_83847.htm]

[21] M. Tedesco, J. Jeyaratnam, and R. Kelly. (2015). *NRT AMSR2 Daily L3 Global Snow Water Equivalent EASE-Grids*. [Online]. Available: http://dx.doi.org/10.5067/AMSR2/A2_DySno_NRT

[22] H. E. Brooks and C. A. Doswell, III, "A comparison of measures-oriented and distributions-oriented approaches to forecast verification," *Weather Forecasting*, vol. 11, pp. 288–303, 1996.

[23] H. Eldardiry, E. Habib, Y. Zhang, and J. Graschel, "Artifacts in stage IV NWS real-time multisensory precipitation estimates and impacts on identification of maximum seriers," *J. Hydrol. Eng.*, vol. 22, no. 5, pp. E015003, 1–13, 2017, doi:10.1061/(ASCE/HE.1943-5584.0001291.

[24] B. R. Nelson, O. P. Prat, D. J. Seo, and E. Habib, "Assessment and implications of NCEP Stage IV quantitative precipitation estimates for product intercomparisons," *Weather Forecasting*, vol. 31, pp. 371–394, 2015. [Online]. Available: http://dx.doi.org/10.1175/WAF-D-14-00112.1

Shuyan Liu received the B.S. and M.S. degrees in atmospheric physics and environment from Nanjing Institute of Meteorology, Nanjing, China, in 2000 and 2003, respectively, and the Ph.D. degree in meteorology from Nanjing University of Information Science and Technology, Nanjing, in 2006.

From 2006 to 2007, she was a Lecturer with Beijing Normal University, Beijing, China. From 2007 to 2011, she was a Model Developer with Illinois State Water Survey, University of Illinois at Urbana-Champaign, Champaign, IL, USA. From 2011 to 2015, she was a Research Associate with the Earth System Science Interdisciplinary Center, University of Maryland, College Park, MD, USA. Since 2015, she has been a Research Scientist II with the Cooperative Institute for Research in the Atmosphere, NOAA center for Satellite Application and Research, National Environmental Satellite, Data, and Information Service, College Park.

Christopher Grassotti received the B.S. degree in earth and space science from the State University of New York, Stony Brook, NY, USA, the M.S. degree in meteorology from the University of Wisconsin-Madison, Madison, WI, USA, and the M.S. degree in viticulture and enology from AgroMontpellier, Montpellier, France, in 1982, 1986 and 2008, respectively.

From 1986 to 1991 and again from 1993 to 2005, he was a a Research Associate and Senior Research Associate with Atmospheric and Environmental Research, Inc. From 1991 to 1993, he was with the Atmospheric Environmental Service, Environment Canada in Dorval, Quebec, Canada. Since 2008, he has been with the National Oceanic and Atmospheric Administration Center for Satellite Application and Research, National Environmental Satellite, Data, and Information Service, College Park, MD, USA.

Junye Chen received the B.S. and M.S. degrees in atmospheric science from Peking University, Beijing, China, in 1995 and 1998, respectively, and the Ph.D. degree in atmospheric science from Columbia University, New York, NY, USA, in 2005.

From 2005 to 2014, he was a Research Associate and Assistant Research Scientist with the Earth System Science Interdisciplinary Center, University of Maryland, College Park, MD, USA. Since 2014, he has been with the NOAA Center for Satellite Application and Research, College Park.

Quanhua Liu received the B.S. degree from Nanjing University of Information Science and Technology (former Nanjing Institute of Meteorology), Nanjing, China, the Master's degree in physics from Chinese Academy of Science, Beijing, China, and the Ph.D. degree in meteorology and remote sensing from the University of Kiel, Kiel, Germany, in 1982, 1984 and 1991, respectively.

He is currently a Physical Scientist with the NOAA Center for Satellite Application and Research, National Environmental Satellite, Data, and Information Service, College Park, MD, USA, and is leading the soundings team at NOAA/STAR. The sounding system utilized satellite-based microwave observations and infrared hyperspectral measurements to acquire vertical profiles of atmospheric temperature, water vapor, ozone, CO, CH_4, CO_2, and others chemical species. He studied the infrared hyperspectral sensor and the Community Radiative Transfer Model (CRTM). The CRTM has been operationally supporting satellite radiance assimilation for weather forecasting. The CRTM also supports JPSS/SNPP and GOES-R missions for instrument calibration, validation, long-term trend monitoring, and satellite retrieved products.

GPM Products From the Microwave-Integrated Retrieval System

Shuyan Liu, Christopher Grassotti, Junye Chen, and Quanhua Liu

***Abstract*—An updated version of the microwave-integrated retrieval system (MiRS) V11.2 was recently released. In addition to the previous capability to process multiple satellites/sensors, the new version has been extended to process global precipitation measurement (GPM) microwave imager (GMI) measurements. The main purpose of this study is to introduce MiRS GPM products and to evaluate rain rate, total precipitable water (TPW), and snow water equivalent (SWE) using various independent datasets. Rain rate evaluations were performed for January, April, July, and October 2015 which represents one full month in each season. TPW was evaluated on four days: 9 January, 1 April, 13 July, and 1 October, which represents one full day in each season. SWE was evaluated for a week in January 2015. Results show that MiRS performance is generally satisfactory in regards to both global/regional geographical distribution and quantified statistical/categorical scores. Histograms show that MiRS GPM rain rate estimates have the capability to reproduce moderate to heavy rain frequency distribution over land, and light rain distribution over ocean when compared with a ground-based reference. Evaluations of TPW show the best performance over ocean with the correlation coefficient, bias, and standard deviation of 0.99, <1.25 mm, and <2.4 mm, respectively. Robust statistical results were also obtained for SWE, with a correlation coefficient, bias, and standard deviation of 0.77, 1.72 cm, and 3.61 cm, respectively. The examples shown demonstrate that MiRS, now extended to GPM/GMI, is capable of producing realistic retrieval products that can be used in broad applications including extreme weather events monitoring, depiction of global rainfall distribution, and water vapor patterns, as well as snow cover monitoring.**

***Index Terms*—Global precipitation measurement (GPM), microwave-integrated retrieval system (MiRS), rain rate (RR), satellite.**

Manuscript received September 2, 2016; revised January 23, 2017, April 3, 2017, and May 22, 2017; accepted June 10, 2017. This work was supported by the NOAA under Grant NA14OAR4320125. *(Corresponding author: Shuyan Liu.)*

S. Liu is with the Cooperative Institute for Research in the Atmosphere, Colorado State University, Fort Collins, CO 80523 USA, and also with the NOAA Center for Satellite Application and Research, National Environmental Satellite, Data, and Information Service, College Park, MD 20740 USA. (e-mail: shu-yan.liu@noaa.gov).

C. Grassotti and J. Chen are with the Cooperative Institute for Climate and Satellites-MD/Earth System Science Interdisciplinary Center, University of Maryland, College Park, MD 20740 USA, and also with the NOAA Center for Satellite Application and Research, National Environmental Satellite, Data, and Information Service, College Park, MD 20740 USA. (e-mail: christopher.grassotti@noaa.gov; junye.chen@noaa.gov).

Q. Liu is with the NOAA Center for Satellite Application and Research, National Environmental Satellite, Data, and Information Service, College Park, MD 20740 USA. (e-mail: quanhua.liu@noaa.gov).

Color versions of one or more of the figures in this paper are available online at http://ieeexplore.ieee.org.

Digital Object Identifier 10.1109/JSTARS.2017.2716356

I. Introduction

Satellite-based observations have provided expanded opportunities for rainfall and hydrometeor monitoring by providing global-scale brightness temperature measurements over land and ocean. Accurate rain rate retrieval around the globe is crucial for applications, such as extreme weather event detection, flood, and drought monitoring. Retrieval techniques based on space-based measurements began in 1970s when meteorological satellites became operational in greater number and began transmitting radiance data back to the Earth [1]. Due to the advantages of high spatial and temporal coverage relative to ground-based measurements, such as radar and rain gauge, many algorithms have been developed to convert satellite measured radiances into geophysical parameters, including precipitation.

By estimating the direct interaction of the radiation with liquid and frozen water in the atmospheric column, data from microwave radiometers, thus, can be used to provide physically reasonable retrievals of precipitation rate. Wilheit *et al.* [2] comprehensively examined 16 rainfall intensity retrieval algorithms including algorithms that use high-frequency scattering measurements, low-frequency emission measurements, and combinations based on the special sensor mircrowave imager radiances. Weng *et al.* [3] and Ferraro *et al.* [4] described the microwave surface and precipitation product system which retrieves total precipitable water (TPW), cloud liquid water, and ice water path using a physical approach, and evaluated the product based on multiple sensors. The advantages of statistical regression-based algorithms are 1) they do not require knowledge of the physical relationship between rain rate and satellite brightness temperature, and 2) assuming there exists a linear relationship between brightness temperatures and rainfall, they always minimize the least squares retrieval error. However, the relationship between rain rate and microwave radiances is known to be highly nonlinear, as well as exhibit seasonal and regional dependence. Thus, a physical-based retrieval algorithm was introduced by Petty [5] aimed at inverting multichannel microwave radiances to determine physical information on hydrometeors. In addition to rain, Surussavadee and Staelin [6] extended the retrievals to snowfall rate and to snow and ice surfaces. The Goddard Profiling Algorithm is a noteworthy system which uses a Bayesian inversion for all surface types. The method was first developed to retrieve precipitation from the tropical rainfall measuring mission microwave imager [7], and then evolved to a fully parametric approach used operationally on global precipitation measurement (GPM) microwave imager (GMI) [8].

The microwave-integrated retrieval system (MiRS, https://www.star.nesdis.noaa.gov/mirs/) is an inversion algorithm based on physical forward modeling and can invert observed multichannel radiances simultaneously to determine key components of the atmosphere and surface state, including rain parameters [9], [10]. The system has been operational since 2007 at the National Oceanic and Atmospheric Administration (NOAA) and has routinely produced satellite retrieval products from a growing list of microwave satellites/sensors. The most recent released version is V11.2 which extended MiRS capability to process GPM/GMI measurements. This study introduces and evaluates GPM/GMI retrieval products within the MiRS framework. Section II introduces 1) the MiRS algorithm, 2) the GPM/GMI data used as input to the system, 3) other datasets that were used as references to estimate performance, and 4) the performance evaluation methods. Section III includes MiRS-retrieved products and evaluation results. Discussion and conclusion are in Section IV.

II. Algorithm, Data, and Evaluation Method

The MiRS is an iterative physically-based one-dimensional variational (1-DVAR) retrieval algorithm [11], [12]. The principle is to minimize a two-term penalty function, which is composed of the departure of the simulated radiances from measurements and the departure of the retrieved parameters from their respective *a-priori* backgrounds. To evaluate MiRS-GPM/GMI products, we used various independent data for different parameters, i.e., Stage-IV radar-gauge composites for rain rate (RR), European Centre for Medium-Range Weather Forecasts (ECMWF) global analyses for TPW, and Japan Aerospace Exploration Agency (JAXA) advanced microwave scanning radiometer 2 (AMSR2) data for snow water equivalent (SWE).

A. MiRS Algorithm

The 1-DVAR algorithm used by MiRS is an iterative approach finding the optimal solution that fits the observed satellite radiance, subject to other constraints. The cost function to be minimized is

$$J(X) = \left[\frac{1}{2}(X - X_0)^T \times B^{-1} \times (X - X_0)\right] + \cdot \left[\frac{1}{2}(Y^m - Y(X))^T \times E^{-1} \times (Y^m - Y(X))\right] \quad (1)$$

where *X* is the retrieved state vector. The first item on the right represents the penalty for departing from background X_0 weighted by the error covariance matrix *B*. The second term represents the penalty for the simulated radiances *Y* departing from the observed radiances Y^m, weighted by instrument and modeling error *E*.

Assuming local linearity

$$y(x) = y(x_0) + K[x - x_0]. \quad (2)$$

This leads to iterative solution

$$\Delta X_{n+1} = \left\{BK_n^T\left(K_n B K_n^T + E\right)^{-1}\right\} \cdot [(Y^m - Y(X_n)) + K_n \Delta X_n] \quad (3)$$

where ΔX is the increment of the state vector iteration $n + 1$, and *K* is the matrix of Jacobian which contains the sensitivity of the radiances to changes in X (parameters to retrieve).

The departure from measured radiances normalized by the noise level and the specification of uncertainty in the forward modeling make it possible to use the signal of a particular channel when the geophysical signature is stronger than the noise. Conversely, at other times, it may be possible to deweight the information from same channel when the signal in question is within the noise level. The departure from the background scaled by the uncertainty assigned to the background result in retrievals closer to an *a-priori* background estimate if it is deemed accurate. The MiRS currently uses a "dynamic background" as an *a-priori* constraint, for temperature, water vapor, and skin temperature, which varies with latitude, longitude, season, and time of day. Empirical orthogonal functions are used as basis functions to further reduce the degrees of freedom in the solution and stabilize the retrieval.

The Community Radiative Transfer Model (CRTM) [13], [14] produces radiances and the corresponding Jacobians under clear, cloudy, and precipitating conditions. The model has been validated against various satellite measurements [15], [16]. MiRS uses CRTM as the forward operator to perform retrievals under all these sky conditions. Given a set of radiances, an *a-priori* (background) estimate of the geophysical mean and its associated covariance matrix, and assuming the hypotheses for its mathematical basis are satisfied, MiRS produces a set of self-consistent parameters that are also consistent with the measured parameters. When processing satellite sensor data with a full complement of temperature, water vapor, and surface-sensitive channels, the official MiRS products generally include temperature and water vapor vertical profiles, cloud and precipitation vertical profiles (nonprecipitating cloud amount, rain, and graupel), skin temperature, and the surface emissivity spectrum. Postprocessing of elements within the retrieved state vector yield additional retrieval products, such as RR, TPW, sea ice concentration and age, SWE, and grain size. In the case of TPW, simple vertical integration of the retrieved water vapor profile is done. For RR, offline relationships between surface RR and total rain water, graupel water, and cloud liquid water path were developed from mesoscale forecast model simulations. Finally, for sea ice and snow water, external catalogs that relate the surface emissivity spectrum to ice and snow amounts are used. In the case of snow water, a single-layer physical snow model developed at NOAA is used to build the catalogs. An important feature of MiRS is that, as currently configured, retrievals do not require real-time ancillary data such as those coming from numerical weather prediction model forecasts. MiRS products based on various satellite/sensors have been examined, for example, [17], [18]. In the case of GPM/GMI, with a reduced channel set primarily designed to measure surface and precipitation phenomena, the official MiRS GPM products are RR, rain water path, graupel water path, cloud liquid water, TPW, and SWE.

B. Datasets Description

The GPM satellite, launched on February 27, 2014, is a joint effort of JAXA and the National Aeronautics and Space Administration. GPM has dual-frequency precipitation radar and GMI passive radiometer onboard. This study uses GMI observed microwave radiances as input to MiRS. GMI, across a swath of 885 km, is a passive sensor that uses 13 different frequency/polarization channels to observe energy from various types of precipitation through clouds for estimating everything from heavy to light rain and for detecting falling snow. Table I lists GMI channel information, including central frequency, polarization, bandwidth, noise equivalent differential temperature (NEDT), beam width, and ground footprint size. Retrieved output products from MiRS analyzed in this study include the surface RR as well as rain water, graupel water, and nonprecipitating cloud water. This paper will evaluate RR, TPW, and SWE with different independent data sources.

RR retrievals are evaluated by Stage IV [19], [20] which is a 4-km gridded precipitation analysis over the conterminous U.S. (CONUS) produced by National Centers for Environmental Prediction. The data are based on the multisensor precipitation estimator analyses known as Stage III which use multisensor data (WSR-88D radar and gauges) and are specified on 4-km polar-stereographic grids produced by the 12 River Forecast Centers. In this paper, we used the hourly products that are collocated with GPM/GMI measurements for validation. The ECMWF (http://www.ecmwf.int/) data which are used to evaluate MiRS performance have 91 vertical levels between the surface and 0.01 hPa. The horizontal resolution is approximately 125 km (spectral truncation T159) and the temporal resolution is 3 h. The ECMWF gridded data were matched to sensor granules for direct comparison. MiRS retrieved SWE was compared with the Level-3 SWE dataset based on observations of AMSR2 [21] onboard JAXA Global Change Observation Mission 1st-Water (GCOM-W) June 2015 and were mapped to 25-km grids in near real-time mode (available at https://lance.nsstc.nasa.gov/amsr2-science/data/level3/daysnow/).

C. Evaluation Methods

Performance of the retrieval system was evaluated both objectively by statistical and categorical scores and subjectively by viewing geographical distribution. Statistical evaluation includes correlation coefficients, biases, standard deviations, and root–mean-square errors. In this study, we use three categorical scores [22] to evaluate RR retrieval. Probability of detection (POD), sometimes called hit rate, represents the ratio of total rain retrievals greater than a threshold divided by total rain observations in Stage IV greater than the same threshold and defined by: POD = (number of rain events correctly retrieved by MiRS)/(total number of Stage-IV observed rain events). False alarm ratio (FAR), the fraction of the all observed no rain events (as defined by a threshold) in which there was a retrieval of rain greater than the same threshold, and is calculated by: FAR = (number of retrieved false alarms)/(total number of Stage IV no rain events). (Note that this is defined in [22] as the Probability of false detection.) The Heidke skill score (HSS) measures the fraction of correct rain retrieval after eliminating those retrievals which would be correct due purely to random chance. Thus, HSS = (correct retrieval proportion−proportion correct by chance)/(total number of observations−proportion correct by chance), in which a perfect score = 1.

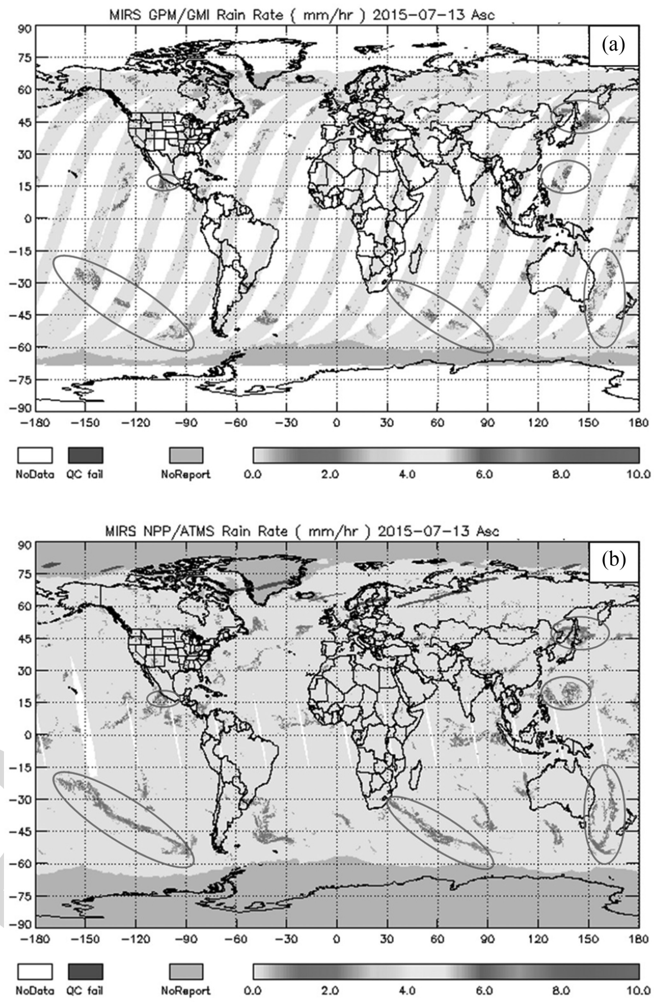

Fig. 1. Global RR distribution intercomparision between (a) MiRS GPM/GMI and (b) SNPP/ATMS for July 13, 2015.

III. Results

The global RR distribution retrieved by MiRS GPM/GMI for July 13, 2015 is shown in Fig. 1(a). MiRS retrievals based on the advanced technology microwave sounder (ATMS) onboard the Suomi national polar-orbiting partnership (SNPP) are also included for an intercomparison (see Fig. 1(b)). MiRS does not retrieve RR over frozen surfaces; thus, the northern and southern snow and sea ice covered areas are denoted as no reports for SNPP/ATMS (see Fig. 1(b)). Despite the swath gaps, GPM/GMI is consistent in distribution and intensity with SNPP/ATMS globally. Active rain areas (red circle on the figures), such as adjacent ocean of southern Mexico and Northern Japan, Philippine

TABLE I
GPM/GMI CHANNEL INFO

Chan. No.	Central Freq. (GHz) (Polarization)	Band Width (MHz)	NEDT[a] (K)	Beam Width (deg)	FOV[b] size AS[c] × CS[d] (km)
1	10.65 (V)	100	0.96	1.75	19.4 × 32.2
2	10.65 (H)	100	0.96	1.75	19.4 × 32.2
3	18.7 (V)	200	0.84	1.00	11.2 × 18.3
4	18.7 (H)	200	0.84	1.00	11.2 × 18.3
5	23.8 (V)	400	1.05	0.90	9.2 × 15
6	36.5 (V)	1000	0.65	0.90	8.6 × 14.4
7	36.5 (H)	1000	0.65	0.90	8.6 × 14.4
8	89.0 (V)	6000	0.57	0.40	4.4 × 7.3
9	89.0 (H)	6000	0.57	0.40	4.4 × 7.3
10	166.0 (V)	3000	1.5	0.40	4.4 × 7.1
11	166.0 (H)	3000	1.5	0.40	4.4 × 7.1
12	183.31 ± 3 (V)	3500	1.5	0.40	4.4 × 7.2
13	183.31 ± 7(V)	4500	1.5	0.40	4.4 × 7.2

[a]NEDT: Noise equivalent differential temperature.
[b]FOV: Field-of-view.
[c]AS: Along-scan direction.
[d]CS: Cross-scan direction.

TABLE II
LAND RR STATISTICAL ANALYSES OVER CONUS

Month	No. of Points ($\times 10^3$)	Corr. Coef.	Bias (mm/h)	Std. Dev. (mm/h)
January	1390	0.60	−0.02	0.58
April	2567	0.55	0.03	0.86
July	2733	0.52	0.04	1.18
October	2662	0.58	0.01	0.70

Sea, the Southern Hemisphere ocean around −45° latitude, etc., are consistent across the two satellite retrievals. There are some inconsistencies between the two due to different local passing time. The SNPP is in a geosynchronous polar orbit with a local equatorial passing time of 1:30 pm (ascending), while GPM orbits between 65°N and 65°S, and does not have a fixed passing time, but one that repeats approximately every two weeks.

RR retrieval performance at the hourly timescale has been quantified for four full months chosen to reflect the typical seasonal cycle over the Northern Hemisphere, which in this study were January, April, July, and October from 2015. Table II contains the statistics based on collocation over the CONUS with the hourly Stage IV analyses over land surfaces. Correlations between land retrievals and observations for January, April, July, and October are 0.60, 0.55, 0.52, and 0.58, biases are −0.02, 0.03, 0.04, and 0.01 mm/h, and the standard deviations are 0.58, 0.86, 1.18, and 0.70 mm/h, respectively.

To characterize the distribution of RR, histograms based on over land rainfall are shown in Fig. 2, for each of the four months. Over land, MiRS typically underestimates relative to Stage IV the occurrence of light rain events below 2.0 mm/h for all four months (see Fig. 2(a)–(d)) with January and July showing the maximum and minimum underestimation, respectively. The seasonal transition months of April and October show similar behavior, lying in between the two extremes of January and July. Above approximately 2 up to 10 mm/h, agreement between MiRS and Stage IV occurrence is quite good in all four months. The underestimation of light rain occurrence over land is characteristic of microwave retrieval algorithms generally, as the emission signal of the rainfall is low relative to the high and variable surface emission background.

We further calculated categorical scores of POD, FAR, and HSS as a function of rain/no rain threshold at 0.5-mm/h intervals. The results are shown in Fig. 3. POD and HSS for the four months are generally higher than 0.3. In July, both POD and HSS are highest at the lowest RR threshold (0.5 mm/h). This is likely due to the climatological presence of low-level stratiform rain in fall, winter, and spring, which can be contrasted with July in which light rainfall may have origins with deeper convective systems having a stronger scattering signal in microwave measurements. Comparing with summer (July) which shows almost linear deceasing scores from light to heavy rain, winter (January) POD, and HSS peaked at 2 mm/h. During spring (April) and fall (October), both PODs have the highest value at 2 mm/h, HSS in April is decreasing with increasing RR while in October is stable between 0.35 and 0.40.

RR retrieval at the regional and monthly scale is illustrated over the CONUS (seeFig. 4) for land surfaces for the same four months in 2015. RR retrievals from GPM were collocated with Stage IV hourly estimates for each day of the month to produce a monthly accumulated rainfall on the Stage IV 4-km grid. (Note that this is not the true monthly accumulation since any location would be sampled at most twice daily by GPM, and because the Stage IV analyses are not reliable for many locations in the mountainous western U.S. due to orographic artifacts in the required radar data [23].) Monthly accumulated rain retrieval along GPM swaths (see Fig. 4(a)–(d)) for January, April, July, and October 2015 is compared with collocated Stage-IV grids (see Fig. 4(e)–(h)). In each map, the areas masked in white over the western U.S. are locations where the Stage IV processing does not estimate rainfall due to radar beam blockage effects. The comparison statistics for the over land estimates are also shown for each month. Generally, the MiRS rainfall retrievals capture major characteristics of the monthly precipitation geographic distribution seen in Stage IV. In January, for example, MiRS GPM and Stage-IV agree very well over the southern

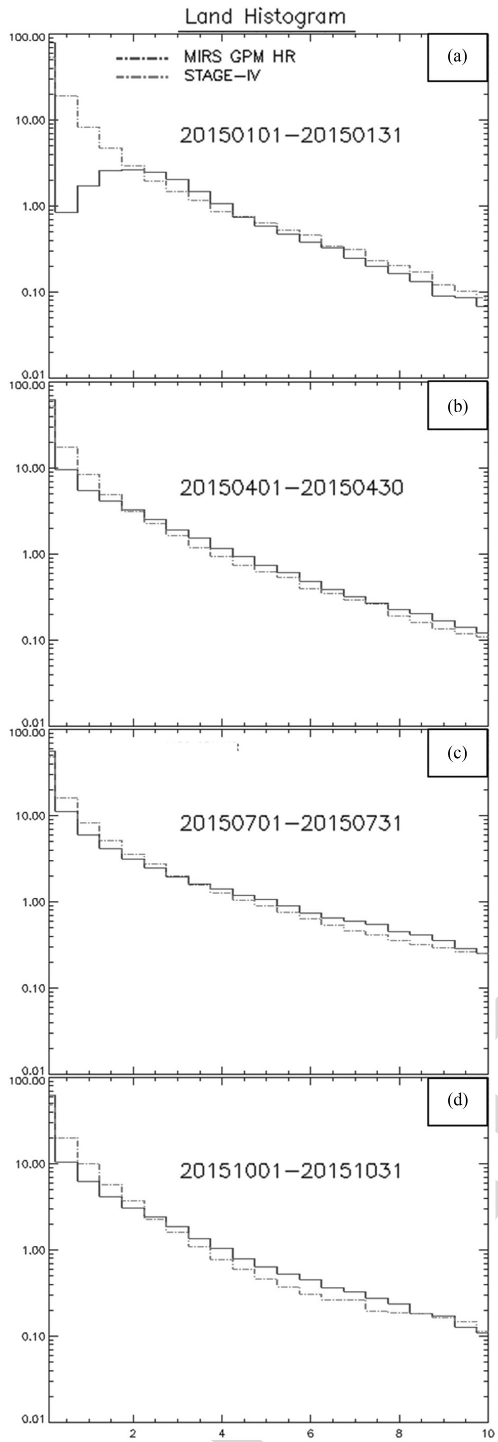

Fig. 2. RR histograms as a function of rain/no rain threshold validated against Stage IV over land for the months of (a) January 2015, (b) April 2015, (c) July 2015, and (d) October 2015.

Gulf Coast states from Texas eastward to the Florida panhandle. Further northward, there is a tendency of the MiRS rainfall to underestimate the totals seen in Stage IV, which is consistent with known difficulties of satellite algorithms to detect and estimate lighter stratiform rainfall common in the cold season (see also Fig. 2(e)–(h)). In the warmer seasons, particularly April and July, the MiRS and Stage IV totals are in fairly good agreement, with some indication that the MiRS amounts at the higher end of the distribution (>100 mm) are more prevalent than those in the Stage IV. The other noticeable feature is the presence during some months of spurious high rainfall amounts at major coastlines and also along some lakeshores such as the Great Lakes. This is due to the presence of mixed surface types within the GMI microwave footprints which are difficult to characterize. Due to the inherently larger size of the measurement footprint relative to infrared observations, microwave rainfall retrieval algorithms often have difficulty with coastlines and many algorithms do not produce estimates if a coastline is detected. The range of comparison statistics over the four months for correlation, bias (mm), and standard deviation (mm) are [0.45, 0.58], [−1.73, 4.25], and [17.6, 28.6], respectively. Total collocation points ranged from 310 289 in January to 404 523 in October.

Finally, it is important to note that the Stage IV data are known to have limitations since radar to RR relationships themselves contains uncertainties and the algorithms used at River Forecast Centers have certain biases. For example, uncertainties increase in the case of light rain detection during winter season generally, and over the Western U.S. as a result of fewer radar locations and mountain beam blockage [24]. This could have the effect of spuriously elevating false alarms and lowering other skill scores when the satellite estimate has correctly identified precipitation.

TPW retrieved from MiRS GPM/GMI was evaluated by comparing with collocated ECMWF analyses. Bias maps from one day in each season, i.e., 9 January, 1 April, 13 July, and 1 October 2015 were shown to illustrate the spatial dependence of retrieval performance (see Fig. 5). In comparison with ECMWF, MiRS generally depicts the geographical distribution of TPW well with larger biases over land than over ocean, snow, and ice for all four days due, in part, to larger uncertainties in land surface emissivity. Thermally cold surfaces have smaller and positive biases than warm surfaces, e.g., the northern hemisphere land compared to the southern hemisphere in January. Northern South America show dry biases all four days, as well as Australia in January and April. For 13 July, TPW over the northern hemisphere land has noticeably large negative biases.

Statistical analyses for land, ocean, snow, and ice surface types were performed separately (see Table III). Among all the surface types, ocean has the highest correlation coefficients of 0.99 regardless of day. Consistent with Fig. 5, land retrievals typically have negative (dry) biases, while other surfaces are smaller and positive. Land and ocean retrievals generally have the highest correlation coefficients, while snow and ice generally show lower correlations. The highly variable nature of cryospheric surface emissivities in space and time, generally contribute to increased uncertainty in retrievals over these surfaces.

Since the MiRS algorithm is run without the use of ancillary data (e.g., NWP-based analyses or forecasts), and since GPM/GMI does not have the full set of temperature sounding channels, it is expected that the water vapor retrievals will have larger uncertainties when compared with measurements from, for example, SNPP/ATMS. Further work on tuning and optimizing some of the constraints in the retrieval system (e.g., atmospheric and surface covariances, radiometric bias

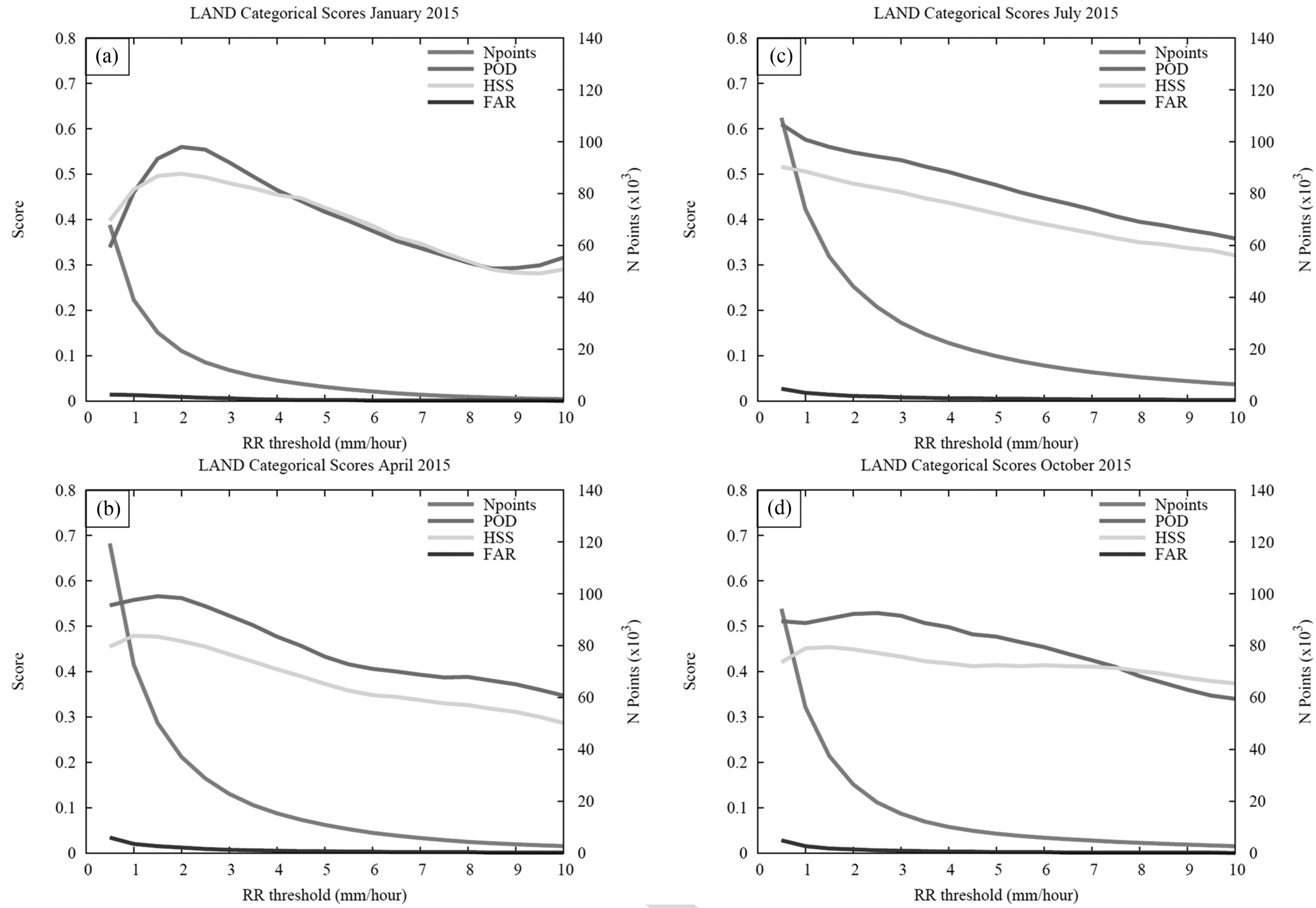

Fig. 3. RR categorical scores as a function of rain/no rain threshold validated against Stage IV over land for the months of (a) January 2015, (b) April 2015, (c) July 2015, and (d) October 2015.

corrections, empirical orthogonal function basis functions) may mitigate some of the biases and uncertainties seen in the retrieved TPW, particularly over land.

Performance of SWE over the northern hemisphere retrievals is shown in Fig. 6. Fig. 6(a) illustrates the northern hemisphere spatial distribution of the MiRS GPM SWE for January 5, 2015, while Fig. 6(b) contains the corresponding map from the independent reference dataset of GCOM-W/AMSR2 SWE, based on the JAXA algorithm. Fig. 6(c) is the density scatter plot of MiRS GPM retrievals and the AMSR2 SWE for one week period of January 4–10, 2015. The two daily maps indicate that in areas with very high SWE, for example, eastern Russia and Siberia, the MiRS GPM estimates tend to be larger than the JAXA AMSR2 estimates, while in areas with lower SWE amounts (<10 cm), for example, Southern Canada and Europe, the MiRS estimates tend to be lower than JAXA AMSR2. Since both products are based on remotely sensed data, it is difficult to state with confidence which estimates may be more accurate. Factors such as snow grain size, forest cover (which tends to mask the underlying snow signal), and local time of observation (which can affect local temperature, and, hence, snow wetness) are all sources of uncertainty in microwave SWE estimates. The scatter plot for the seven-day period shows a distribution of points close to the 1:1 line with a correlation coefficient value of 0.77. Overall, MiRS retrievals are systematically higher than the JAXA AMSR2 estimates (with the regional exception noted above over Asia for the single day). The bias and standard deviation are 1.7 and 3.6 cm, respectively. Comparison statistics for each individual day (not shown) indicate that the results are quite stable and quite close to the aggregate statistics from the one week of processed data. The correlation coefficient ranged from 0.76 to 0.79, bias ranged from 1.5 to 2.2 cm, and standard deviation from 3.6 to 3.7 cm.

IV. Discussion and Summary

MiRS is a robust flexible satellite retrieval system designed for rapid physically-based atmospheric and surface property retrievals from passive microwave measurements. The MiRS algorithm has been running operationally at NOAA since 2007 and routinely distributing satellite derived products through NOAA Office of Satellite and Product Operations. The system is now processing multiple satellites/sensors, i.e., AMSUA and MHS onboard NOAA-18, NOAA-19, MetopA, and MetopB which are polar-orbiting operational environmental satellites; ATMS onboard SNPP satellite; special sensor microwave imager/sounder onboard defense meteorological satellite program satellites F-17 and F-18; and sounder for probing vertical profiles of humidity onboard Megha-Tropiques.

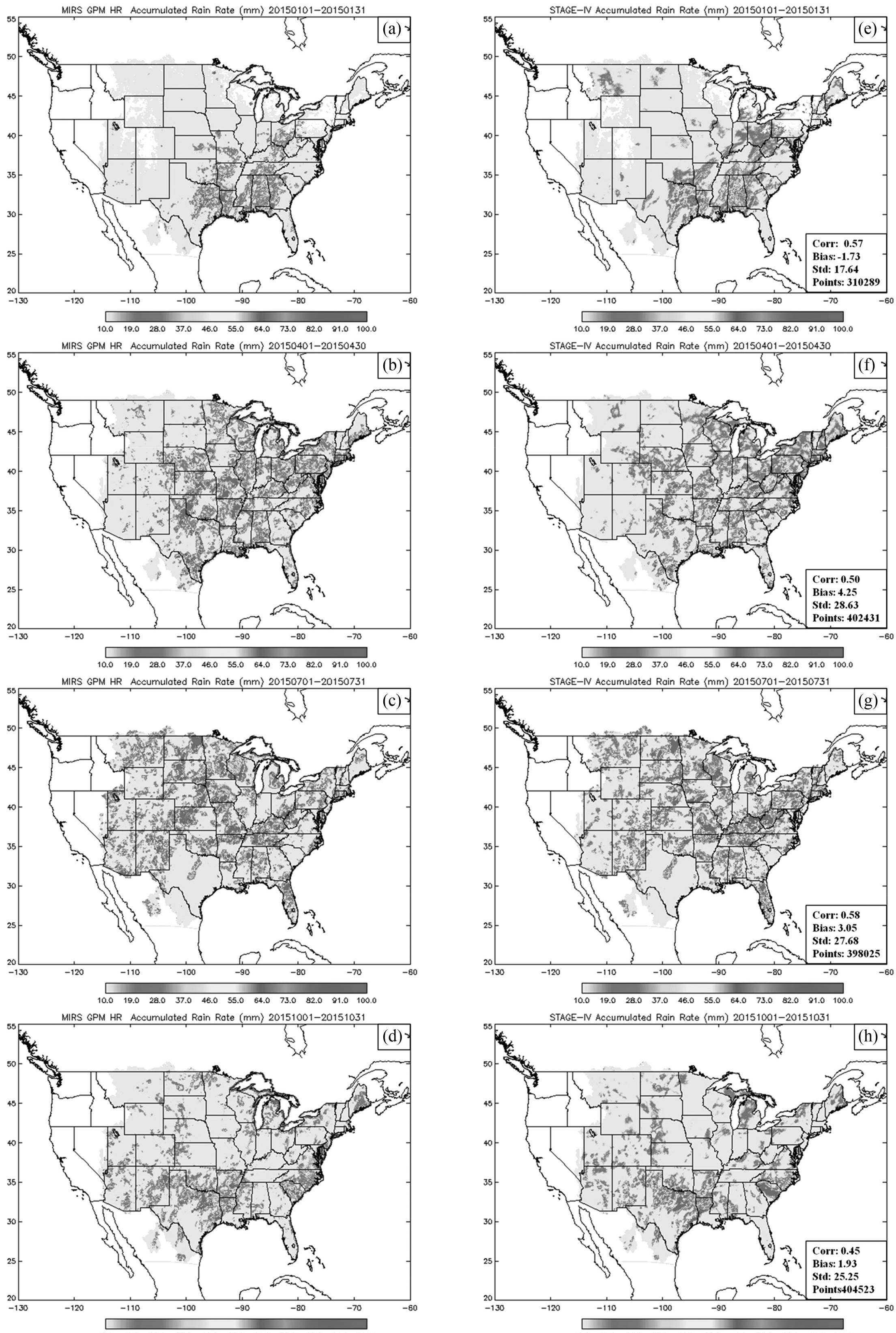

Fig. 4. Accumulated rain (mm) from MiRS GPM/GMI (left panels) and observations from collocated Stage IV (right panels) for the months of (a) and (e) January, (b) and (f) April, (c) and (g) July, and (d) and (h) October 2015. Areas in western U.S. are missing since no Stage IV estimates were produced over these regions. Areas over Rocky Mountains and northern U.S. in January are missing due to frequent snow cover during which MiRS does not produce a rain retrieval.

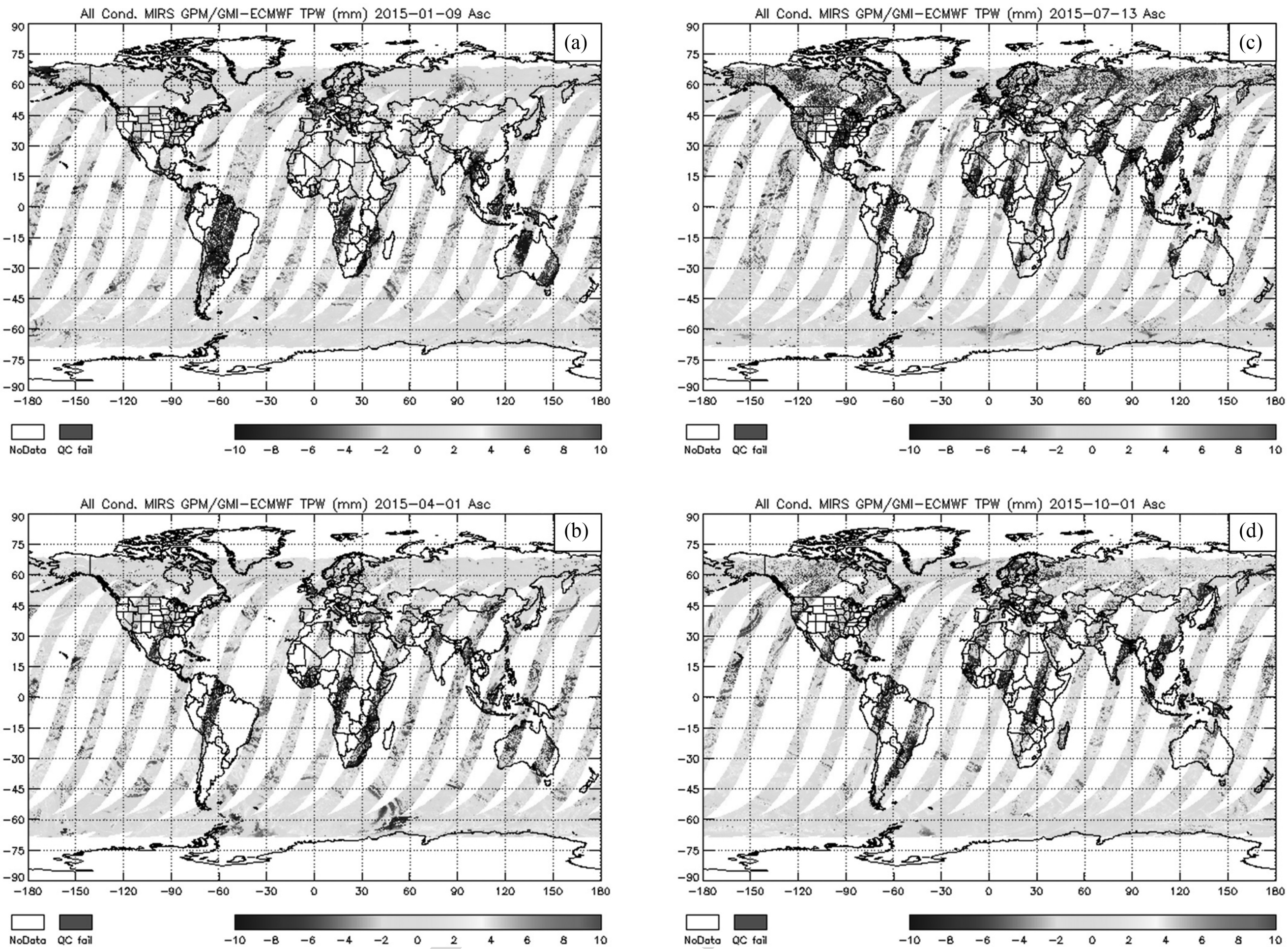

Fig. 5. Geographical distribution of total precipitable water (TPW) biases uses ECMWF as reference for (a) January 9, 2015, (b) April 1, 2015, (c) July 13, 2015, and (d) October 1, 2015.

TABLE III
CLEAR SKY TPW STATISTICAL ANALYSES

Surface Surface	Date Date	No. of Points ($\times 10^3$)	Corr. Coef.	Bias (mm)	Std. Dev. (mm)
Land	2015-01-09	604	0.92	−2.53	6.89
	2015-04-01	542	0.91	−1.76	5.99
	2015-07-13	830	0.83	−1.60	7.04
	2015-10-01	784	0.90	−1.16	6.27
Ocean	2015-01-09	1557	0.99	1.17	2.21
	2015-04-01	1559	0.99	1.17	2.31
	2015-07-13	1534	0.99	1.11	2.38
	2015-10-01	1502	0.99	1.24	2.17
Snow	2015-01-09	458	0.86	0.36	1.44
	2015-04-01	348	0.82	0.72	1.62
	2015-07-13	26	0.82	0.89	3.05
	2015-10-01	57	0.66	1.23	2.53
Ice	2015-01-09	138	0.74	0.29	2.46
	2015-04-01	114	0.72	0.13	2.59
	2015-07-13	234	0.91	0.11	1.97
	2015-10-01	277	0.85	0.84	1.55

The most recent version (v11.2) has been extended to GPM/GMI. This study is intended as an introductory quantitative assessment of the MiRS GPM retrieval products of RR, TPW, and SWE using independent datasets. Global and regional CONUS geographical distribution of surface precipitation is in good qualitative agreement with SNPP/ATMS retrievals and with the operational Stage-IV analyses. Quantitative evaluation based on four months (one full month in each season) showed that MiRS GPM RR performance is consistent with that seen for MiRS RR from other operational satellites. TPW distribution is consistent with ECMWF globally with higher biases over land than over ocean based on the four days (one day in each season) of evaluation. As expected, among the four surface types, ocean TPW has the best performance. This is consistent with TPW performance seen from MiRS for other sensors and from other microwave algorithms. SWE over northern hemisphere was compared with the corresponding product based on AMSR2. Point to point comparison indicates good agreement between the two.

Further investigations are underway including 1) evaluating the impact of assumed radiometric uncertainty in each channel, 2) influence of each assumed *a-priori* hydrometeor background constraints, 3) possible implementation of an *a-priori* temperature and water vapor error covariance matrix specific to rainy conditions, 4) exploring methods to distinguish convective and stratiform (or mixed) precipitation types using, when available,

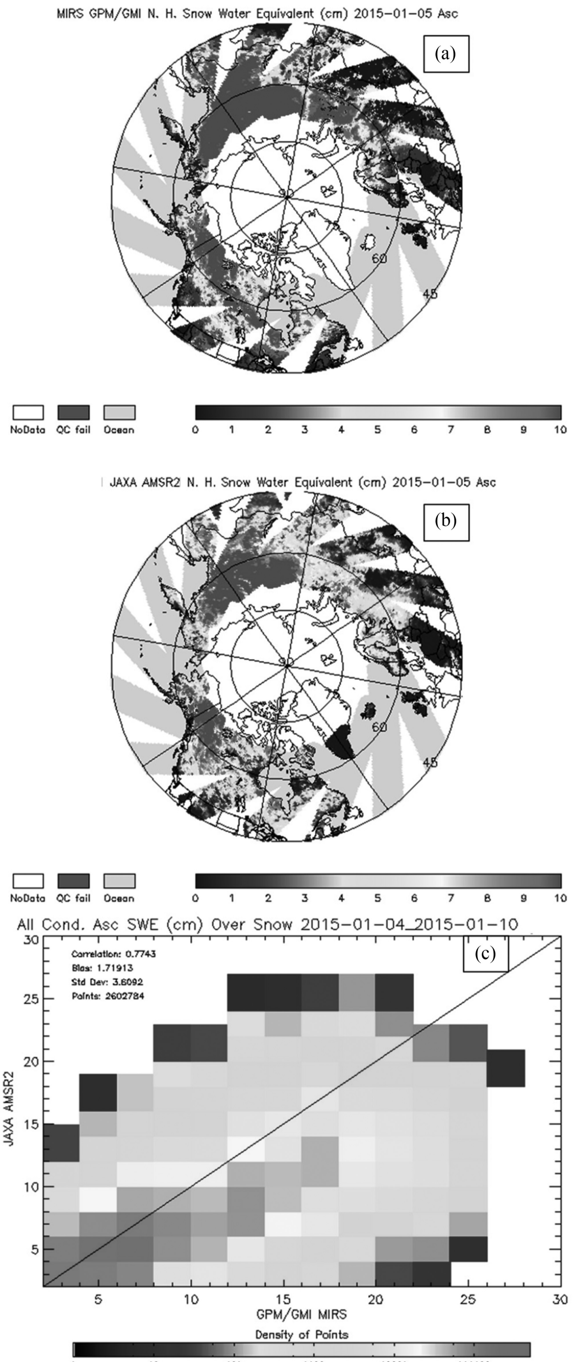

Fig. 6. SWE distribution over the northern hemisphere retrieved from (a) MiRS GPM, (b) AMSR2 retrieval from JAXA algorithm for January 5, 2015, and (c) density scatter plot for one week of January 4–10, 2015.

signal differences between measurements in vertical and horizontal polarization, and 5) use of an air mass-dependent set of radiometric bias corrections instead of the current static corrections. One of the important features of MiRS is that when run in operations, it does not use any ancillary data. External data for the surface (especially emissivity) from climatology or for the atmosphere (water vapor, temperature) from numerical weather prediction systems is anticipated to be beneficial to the retrieval products, but needs to be quantified. Another improvement path in MiRS is that particle size assumptions in CRTM may not be optimal for all precipitation types (e.g., seasonal, regional, stratiform versus convective). Finally, the impact of updated scattering tables (to be available in upcoming versions of CRTM) that account for the effects of nonspherical particles will need to be evaluated.

ACKNOWLEDGMENT

This paper contents are solely the opinions of the authors and do not constitute a statement of policy, decision, or position on behalf of NOAA or the U.S. Government.

REFERENCES

[1] P. A. Arkin and B. N. Meisner, "The relationship between large-scale convective rainfall and cold cloud over the western hemisphere during 1982-84," *Monthly Weather Rev.*, vol. 115, no. 1, pp. 51–74, Jan. 1987.
[2] T. T. Wilheit *et al.*, "Algorithms for the retrieval of rainfall from passive microwave measurements," *Remote Sens. Rev.*, vol. 11, nos. 1–4, pp. 163–194, Oct. 2004.
[3] F. Weng, L. Zhao, R. R. Ferraro, G. Poe, X. Li, and N. C. Grody, "Advanced microwave sounding unit cloud and precipitation algorithms," *Radio Sci.*, vol. 38, no. 4, pp. 8068–8081, Mar. 2003, doi:10.1029/2002RS002679.
[4] R. R. Ferraro *et al.*, "NOAA operational hydrological products derived from the advanced microwave sounding unit," *IEEE Trans. Geosci. Remote Sens.*, vol. 43, no. 5, pp. 1036–1049, May 2005, doi:10.1109/TGRS.2004.843249.
[5] G. W. Petty, "Physical retrievals of over-ocean rain rate from multichannel microwave imagery. Part II: Algorithm implementation," *Meteorol. Atmos. Phys.*, vol. 54, nos. 1–4, pp. 101–121, Mar. 1994.
[6] C. Surussavadee and D. H. Staelin, "Satellite retrievals of arctic and equatorial rain and snowfall rates using millimeter wavelengths," *IEEE Trans. Geosci. Remote Sens.*, vol. 47, no. 11, pp. 3697–3707, Nov. 2009.
[7] C. D. Kummerow *et al.*, "The evolution of the goddard profiling algorithm (GPROF) for rainfall estimation from passive microwave sensors," *J. Appl. Meteorol.*, vol. 40, no. 11, pp. 1801–1820, Nov. 2001.
[8] C. D. Kummerow *et al.*, "The evolution of the goddard profiling algorithm to a fully parametric scheme," *J. Atmos. Ocean. Technol.*, vol. 32, pp. 2265–2280, Dec. 2015.
[9] S.-A. Boukabara, F. Weng, and Q. Liu, "Passive microwave remote sensing of extreme weather events using NOAA-18 AMSUA and MHS," *IEEE Trans. Geosci. Remote Sens.*, vol. 45, no. 7, pp. 2228–2246, Jul. 2007.
[10] S.-A. Boukabara *et al.*, "MiRS: An all-weather 1DVAR satellite data assimilation & retrieval system," *IEEE Trans. Geosci. Remote Sens.*, vol. 49, no. 9, pp. 3249–3272, Sep. 2011, doi:10. 1109/TGRS.2011.2158438.
[11] C. D. Rodgers, *Inverse Methods for Atmospheric Sounding: Theory and Practice*. Singapore: World Scientific, 2000.
[12] Q. Liu and F. Weng, "One-dimensional retrieval algorithm of temperature, water vapor, and cloud water profiles from advanced microwave sounding unit (AMSU)," *IEEE Geosci. Remote Sens.*, Seoul, Korea, vol. 43, no. 5, pp. 1087–1095, 2005.
[13] F. Weng *et al.*, "JCSDA community radiative transfer model (CRTM)," in *Proc. 14th TOVS Conf.*, Beijing, China, 2005, pp. 217–222.
[14] Y. Han *et al.*, "Community radiative transfer model (CRTM)," Dept. Commerce, NOAA, Washington, DC, USA, Tech. Rep. 122, 2006.
[15] Y. Chen, F. Weng, Y. Han, and Q. Liu, "Validation of the community radiative transfer model (CRTM) by using CloudSat data," *J. Geophys. Res.*, vol. 113, no. D8, pp. 2156–2202, 2008.
[16] S. Ding *et al.*, "Validation of the community radiative transfer model," *J. Quant. Spectrosc. Radiat. Transf.*, vol. 112, no. 6, pp. 1050–1064, 2011.
[17] S.-A. Boukabara *et al.*, "A physical approach for a simultaneous retrieval of sounding, surface, hydrometer, and cryospheric parameters from SNPP/ATMS," *J. Geophys. Res. Atmos.*, vol. 118, no. 12, pp. 12 600–12 619, 2013, doi:10.002/2013JD020448.
[18] F. Iturbide-Sanchez *et al.*, "Assessment of a variational inversion system for rainfall rate over land and water surfaces," *IEEE Trans. Geosci. Remote Sens.*, vol. 49, no. 9, pp. 3311–3333, Sep. 2011, doi:10.1109/TGRS.2011.2119375.

[19] M. E. Baldwin and K. E. Mitchell, "Progress on the NCEP hourly multisensory U.S. precipitation analysis for operations and GCIP research," in *Proc. Amer. Meteor. Soc. 2nd Symp. Integr. Obs. Syst.*, Phoenix, AZ, USA, 1998, pp. 54–55.

[20] Y. Lin and K. E. Mitchell, "The NCEP stage II/IV hourly precipitation analyses: Development and applications," in *Proc. Amer. Meteor. Soc. 19th Conf. Hydrol.*, San Diego, CA, USA, 2005, Paper 1.2. [Online]. Available: http://ams.confex.com/ams/Annual2005/techprogram/paer_83847.htm]

[21] M. Tedesco, J. Jeyaratnam, and R. Kelly. (2015). *NRT AMSR2 Daily L3 Global Snow Water Equivalent EASE-Grids*. [Online]. Available: http://dx.doi.org/10.5067/AMSR2/A2_DySno_NRT

[22] H. E. Brooks and C. A. Doswell, III, "A comparison of measures-oriented and distributions-oriented approaches to forecast verification," *Weather Forecasting*, vol. 11, pp. 288–303, 1996.

[23] H. Eldardiry, E. Habib, Y. Zhang, and J. Graschel, "Artifacts in stage IV NWS real-time multisensory precipitation estimates and impacts on identification of maximum seriers," *J. Hydrol. Eng.*, vol. 22, no. 5, pp. E015003, 1–13, 2017, doi:10.1061/(ASCE/HE.1943-5584.0001291.

[24] B. R. Nelson, O. P. Prat, D. J. Seo, and E. Habib, "Assessment and implications of NCEP Stage IV quantitative precipitation estimates for product intercomparisons," *Weather Forecasting*, vol. 31, pp. 371–394, 2015. [Online]. Available: http://dx.doi.org/10.1175/WAF-D-14-00112.1

Shuyan Liu received the B.S. and M.S. degrees in atmospheric physics and environment from Nanjing Institute of Meteorology, Nanjing, China, in 2000 and 2003, respectively, and the Ph.D. degree in meteorology from Nanjing University of Information Science and Technology, Nanjing, in 2006.

From 2006 to 2007, she was a Lecturer with Beijing Normal University, Beijing, China. From 2007 to 2011, she was a Model Developer with Illinois State Water Survey, University of Illinois at Urbana-Champaign, Champaign, IL, USA. From 2011 to 2015, she was a Research Associate with the Earth System Science Interdisciplinary Center, University of Maryland, College Park, MD, USA. Since 2015, she has been a Research Scientist II with the Cooperative Institute for Research in the Atmosphere, NOAA center for Satellite Application and Research, National Environmental Satellite, Data, and Information Service, College Park.

Christopher Grassotti received the B.S. degree in earth and space science from the State University of New York, Stony Brook, NY, USA, the M.S. degree in meteorology from the University of Wisconsin-Madison, Madison, WI, USA, and the M.S. degree in viticulture and enology from AgroMontpellier, Montpellier, France, in 1982, 1986 and 2008, respectively.

From 1986 to 1991 and again from 1993 to 2005, he was a a Research Associate and Senior Research Associate with Atmospheric and Environmental Research, Inc. From 1991 to 1993, he was with the Atmospheric Environmental Service, Environment Canada in Dorval, Quebec, Canada. Since 2008, he has been with the National Oceanic and Atmospheric Administration Center for Satellite Application and Research, National Environmental Satellite, Data, and Information Service, College Park, MD, USA.

Junye Chen received the B.S. and M.S. degrees in atmospheric science from Peking University, Beijing, China, in 1995 and 1998, respectively, and the Ph.D. degree in atmospheric science from Columbia University, New York, NY, USA, in 2005.

From 2005 to 2014, he was a Research Associate and Assistant Research Scientist with the Earth System Science Interdisciplinary Center, University of Maryland, College Park, MD, USA. Since 2014, he has been with the NOAA Center for Satellite Application and Research, College Park.

Quanhua Liu received the B.S. degree from Nanjing University of Information Science and Technology (former Nanjing Institute of Meteorology), Nanjing, China, the Master's degree in physics from Chinese Academy of Science, Beijing, China, and the Ph.D. degree in meteorology and remote sensing from the University of Kiel, Kiel, Germany, in 1982, 1984 and 1991, respectively.

He is currently a Physical Scientist with the NOAA Center for Satellite Application and Research, National Environmental Satellite, Data, and Information Service, College Park, MD, USA, and is leading the soundings team at NOAA/STAR. The sounding system utilized satellite-based microwave observations and infrared hyperspectral measurements to acquire vertical profiles of atmospheric temperature, water vapor, ozone, CO, CH_4, CO_2, and others chemical species. He studied the infrared hyperspectral sensor and the Community Radiative Transfer Model (CRTM). The CRTM has been operationally supporting satellite radiance assimilation for weather forecasting. The CRTM also supports JPSS/SNPP and GOES-R missions for instrument calibration, validation, long-term trend monitoring, and satellite retrieved products.